Gliogenesis from the subventricular zone modulates the extracellular matrix at the glial scar after brain ischemia

Maria Ardaya[1,2,3,9], Marie-Catherine Tiveron[4], Harold Cremer[4], Benjamin Dehay[5], Fernando Pérez-Cerdá[1,2,3], Carlos Matute[1,2,3], Federico N. Soria[1,2,3,6,*], Fabio Cavaliere[1,2,3,7,8,*]

[1]Achucarro Basque Center for Neuroscience, Leioa, Spain.

[2]Department of Neuroscience, University of the Basque Country (UPV/EHU), Leioa, Spain.

[3]CIBERNED, Madrid, Spain.

[4]Aix Marseille Univ, CNRS, IBDM, Campus de Luminy, Marseille, France.

[5]Univ. Bordeaux, CNRS, IMN, UMR 5293, F-33000 Bordeaux, France.

[6]Ikerbasque, Basque Foundation for Science, Bilbao, Spain.

[7]Basque Biomodel Platform for Human Research (BBioH), Leioa, Spain.

[8]Current Address: Instituto Biofisika (CSIC, UPV/EHU), Fundación Biofísica Bizkaia, Leioa, Spain

[9]Current Address: Donostia International Physics Center (DIPC), San Sebastian, Spain.

[*]Correspondence to fabio.cavaliere@ehu.eus (F.C.), federico.soria@achucarro.org (F.N.S.)

ABSTRACT

Activation of the subventricular zone (SVZ) after cerebral ischemia is one of the early responses in the brain to counteract the loss of neurons and reduce tissue damage. Impaired brain regions communicate with the SVZ through many chemotactic messages that result in neural stem cells (NSC) migration and differentiation. However, the activation of gliogenesis and the role of newborn astrocytes in the post-ischemic scenario is still under debate. We have previously shown that adenosine release after brain ischemia prompts the SVZ to generate new astrocytes. Here, we use transient brain ischemia in mice to define the cellular origin of these astrocytes in the SVZ neurogenic niche and investigate their role in the pathological process. By combining immunofluorescence, BrdU-tracing and genetic cellular labelling, we tracked the migration of newborn astrocytes, positive for the proteoglycan marker Thbs4, from the dorsal and medial SVZ to the perilesional barrier surrounding the ischemic core, termed "glial scar". We found that these Thbs4-positive astrocytes modulate the dense extracellular matrix at the lesion border by synthesis but also degradation of hyaluronan. We also show that while the accumulation of this polymer at the lesion is sufficient to recruit newborn astrocytes, its degradation at the SVZ correlates with gliogenesis. These results point to newborn astrocytes as a plausible pharmacological target to modulate the glial scar after brain ischemia and facilitate tissue regeneration.

INTRODUCTION

Cell regeneration in the adult mammalian brain occurs mainly in two neurogenic niches: the subventricular zone (SVZ) in the lateral ventricle and the subgranular zone (SGZ) in the dentate gyrus of the hippocampus (Bond et al., 2015). Adult brain stem cells are multipotent and derive from the embryonic radial glia, thus sharing the principal cell markers and features with resident astrocytes. In the adult mouse brain, neuroblasts from SVZ migrate through the rostral migratory stream (RMS) to the olfactory bulb (OB), where neurogenesis occurs (Luskin, 1993). Neuronal hyperactivity (e.g., during epilepsy), as well as pathological (e.g., stroke) or natural (e.g., aging) processes, can impair the physiological machinery of the neurogenic niches altering their neurogenic and gliogenic potential (Chaker et al., 2016; Kralic et al., 2005; Sundholm-Peters et al., 2005). It is known, for instance, that SVZ cells are activated *in vivo* after focal ischemia following a middle cerebral artery occlusion (MCAO) (Ceanga et al., 2021).

We have previously demonstrated in oxygen and glucose-deprived (OGD) organotypic brain slices that the ischemic region and the SVZ establish a biochemical interplay based on a gradient of toxic and protective factors released early after the insult (Cavaliere et al., 2006). Furthermore, others have demonstrated that brain stroke models in mice can activate astrogliogenesis to the detriment of neurogenesis (Benner et al., 2013; Laug et al., 2019; Li et al., 2010; Young et al., 2012). Benner and colleagues identified an SVZ-derived astrocyte population characterized by high levels of the membrane-bound proteoglycan thrombospondin 4 (Thbs4), a cell-cell and cell-matrix adhesion molecule that has been deemed neuroprotective against ischemic damage (Benner et al., 2013; Laug et al., 2019). Ablation of Thbs4 in KO mice also produced abnormal ischemic scar formation and increased microvascular haemorrhage, suggesting a role of SVZ astrogliogenesis in brain damage and glial scar formation induced by ischemic stroke (Benner et al., 2013).

The perilesional barrier known as the *glial scar* assembles early after brain ischemia, isolating the damaged area and constraining both the spread of pathogens and potentially toxic damage-associated molecular patterns (DAMPs) into the surrounding area (Anderson et al., 2016; Bush et al., 1999;

Faulkner et al., 2004). Consisting of packed reactive astrocytes and a dense extracellular matrix comprised mostly of hyaluronic acid (HA), the glial scar represents a physical barrier for the SVZ-generated newborn neurons which migrate into the ischemic core (Arvidsson et al., 2002; Yamashita et al., 2006). Thus, the modulation of glial scar formation after brain ischemia may represent a strategy to reduce tissue damage and reestablish brain functionality. In ischemic stroke, the brain extracellular matrix (ECM) suffers a thorough restructuration due to injury and must undergo successful remodelling to encourage brain repair. ECM elements involved in the ischemic cascade induce activation of astrocytes and microglia, modulating ECM structure by releasing glycoproteins to the extracellular space (Adams and Gallo, 2018; Fawcett, 2015). This crosstalk culminates in the formation of the glial scar, which is created locally by reactive astrocytes and astrocytes-secreted ECM molecules such as HA and chondroitin sulphate proteoglycans (Bush et al., 1999; Lau et al., 2013).

We have previously demonstrated that high extracellular adenosine levels, a hallmark of ischemic insults, induced astrogliogenesis from the SVZ (Benito-Muñoz et al., 2016). Following our previous results, here we characterized the SVZ response to brain ischemia and investigated the role of newly generated astrocytes in the modulation of the glial scar after MCAO. We show that ischemic conditions increase the number of newly generated astrocytes in the SVZ and their migration to the ischemic area. We also propose the role of these astrocytes in modulating the extracellular matrix at the glial scar and suggest this astrocyte population as a possible target for brain repair after brain ischemia

RESULTS

Thbs4 is expressed in the neurogenic niche of the SVZ.

As suggested by others (Benner et al., 2013; Girard et al., 2014; Pous et al., 2020), Thbs4 is highly expressed in astrocytes of the SVZ and RMS and might have a role in ischemia-induced neurogenesis. To confirm these observations, we labelled the mouse SVZ by immunofluorescence for Thbs4. Thbs4 was mainly expressed in the SVZ, RMS and OB but also in the cerebellum and ventral tegmental area

(Fig. 1A). In the SVZ, the staining was associated with cells with different morphologies (Fig. 1B), ranging from cells with small primary apical processes in contact with the ventricle, to rounded NSC-like cells in the dorsolateral SVZ horn. After quantification by direct count of Thbs4-positive cells, Thbs4-positive astrocytes represented 21,4% of the total SVZ cells (Fig. 1C), with more than 60%of them displaying a radial glia-like type-B morphology (Bond et al., 2015; Doetsch et al., 1999) (Fig. 1D). To confirm Thbs4 expression, we labelled the SVZ cells with the green fluorescent protein (GFP) under the control of the Thbs4 promoter (pThbs4-eGFP) by postnatal (P1) electroporation (Fig. 1E). Twenty-four hours after electroporation, almost 20% of total cells in the dorsal SVZ expressed GFP (Fig. 1F), with a greater extent in the rostral SVZ (Fig. 1G), confirming that Thbs4-positive cells were mainly localized in the neurogenic niche of the SVZ.

Thbs4 expression in the SVZ increases after brain ischemia

To investigate if brain ischemia could activate astrogliogenesis in the SVZ, we analyzed cell proliferation and Thbs4 expression in the SVZ after MCAO. Sixty minutes of MCAO (Fig. S1A) caused neuronal damage in the cortex and striatum, as observed by cresyl violet staining (Fig. S1B) and NeuN immunofluorescence (Fig. S1C). The survival rate at 28 days post-lesion was around 50% (Fig. S1D). Moreover, motor deficits and animal weight of ischemic mice were followed every day after MCAO for 30 days. Motor deficits ameliorated overtime, while body weight dropped sharply the first 3 days after MCAO and was partially restored at 30 dpi (Fig. S1E-F).

To study cell proliferation in the SVZ, we administrated 50 mg/kg BrdU i.p. every two hours (3 doses in total) the day before MCAO (Fig. S2A). We observed an increase of total SVZ BrdU-positive cells 24h after MCAO (Fig. S2B-C). Ki67 immunofluorescence of SVZ wholemount preparations (Fig. S2D) also revealed more than tenfold increase of proliferative cells 24h after MCAO (Fig. S2E). In addition, we observed a significant increase in cleaved Caspase3-positive cells 24h post-lesion (Fig. S2F-G). These results suggest a fast and specific proliferative response in the ischemia-induced SVZ.

We next analyzed Thbs4 staining in combination with Nestin, an NSC marker, and Doublecortin (DCX), a marker of neuroblasts, before and after MCAO. SVZ was analyzed in sham and ischemic mice 7-, 15- and 30-days post-ischemia (dpi). The immunofluorescence analysis of the SVZ (Fig. 2A) showed a transient decrease of Nestin and DCX-positive cells but an increase of Thbs4-positive astrocytes up to 15 dpi (Fig. 2B-D) with respect to the Sham animals. The increase of Thbs4 astrocytes was also confirmed by Western blot analysis using SVZ homogenates (Fig. 2E-F), evidencing a 2-fold increased expression of Thbs4 in the ischemic SVZ. Similarly to immunofluorescence, Western blot also showed decreased Nestin protein levels at 15 dpi (Fig. 2G). These results suggest that Thbs4 expression in the SVZ is increased after ischemia.

Ischemia induces Thbs4-positive newborn astrocytes from SVZ slow proliferative cells

To characterize the different cell populations of the SVZ activated after focal ischemia, we labelled the whole pool of proliferating cells with 1% of BrdU in drinking water for 14 days before MCAO (Codega et al., 2014). One month after MCAO, BrdU in the SVZ mainly stained slow proliferative cells like type B cells, whereas in rapid transit-amplifying cells (type C), BrdU was diluted away. Therefore, we chose to label type C cells by intraperitoneal administration (50 mg/kg) of 5-Iodo-2′-deoxyuridine (IdU) 24h before euthanasia (Fig. 3A). To identify the cell origin of newborn astrocytes, we analyzed the SVZ 30 dpi by immunofluorescence co-labelling Thbs4 and GFAP together with BrdU or IdU. We found a 2-fold increase of the total amount of proliferative cells (BrdU-positive) after MCAO respect to sham group (Fig. 3B), whereas we did not observe a significant change in the number of IdU-positive cells (Fig. 3C). The number of slow proliferative NSC (Thbs4/GFAP/BrdU) increased linearly after MCAO (Fig. 3D, E) especially in the dorsal region of the SVZ (Fig. S3A), whereas the number of activated NSC (Thbs4/GFAP/IdU) did not change significantly either in the whole SVZ (Fig. 3F) or in any subregion analyzed (Fig. S3B). These results suggest that, after ischemia, Thbs4-positive astrocytes derive from the slow proliferative type B cells.

Ischemia-induced newborn astrocytes migrate from the dorsal SVZ to ischemic regions

To confirm that Thbs4-positive astrocytes derived from type B cells of dorsal SVZ, we labelled NSCs of dorsal SVZ by electroporating the pCAGGSx-CRE plasmid in P1 Ai14 Rosa26-CAG-tdTomato transgenic mice (Fig. 4A). Plasmid electroporation induced the expression of tdTomato (tdTOM) by Cre recombination, enabling the spatial tracking and cell fate assessment of electroporated NCS from the dorsal SVZ. 3-4 months after electroporation, we performed the MCAO and tdTOM fluorescence was analyzed at 7, 30 and 60 dpi. To confirm the efficient labelling of NSCs by the electroporation protocol, we followed the tdTOM fluorescence in the OB (Fig. S4A, see methods). Only those animals with tdTOM-positive cells in the OB were taken into account for later analysis. After quantification of tdTOM-positive NSCs 7, 30 and 60 dpi, we observed a significant decrease in tdTOM-positive cells in ischemic animals in all SVZ regions analyzed (Fig. 4B-C and Fig S4B), suggesting that they either left the area, or died. On the contrary, there was a general increase of tdTOM-positive cells outside the SVZ (Fig. 4D-E), especially in the intermediate and caudal axis of the whole brain respect to sham animals (Fig. S4D-G), suggesting that electroporated cells had migrated away from the SVZ.

To identify the proportion of NSCs that differentiated to Thbs4-positive astrocytes following ischemia, we analyzed the co-expression of Thbs4 with tdTOM after MCAO. Despite the general decrease of tdTOM-positive cells in the SVZ, the fraction of Thbs4/tdTOM cells increased at 30 dpi after MCAO (Fig. 4F-G), reaching a maximum increase at 60 dpi (Fig. 4H), in particular in rostral and intermediate SVZ (Fig. S4C). Finally, we analyzed the Thbs4-positive astrocytes recruitment to the ischemic regions. More than half of the total tdTOM-positive cells in the infarcted area expressed the Thbs4 marker at 60 dpi (Fig. 4I-J). These results suggest that ischemia-induced astrogliogenesis in the SVZ occurs in type B cells from the dorsal region, and that these newborn Thbs4-positive astrocytes migrate to the ischemic areas.

Thbs4-positive astrocytes accumulate at the glial scar after brain ischemia.

Nestin, besides its role in the neurogenic niches, is also rapidly and locally expressed by reactive astrocytes and participates in the glial scar formation (Frisén et al., 1995). Thus, we used Nestin immunofluorescence as a reliable tool to identify the lesion border where the glial scar occurs (Fig. 5A). Nestin staining of the scar was also compared with more classical methodologies like TTC staining (Fig. 5B), where viable tissue is stained red and dead tissue is left unstained. The white-pale pink area was then measured as infarct tissue by TTC staining (Fig. 5C). Unlike the TTC staining, which can only be performed hours after the lesion (the infiltration of peripheral immune cells avoids the exposure of the stained area), the visualization of the glial scar with Nestin immunofluorescence allowed us to analyze the lesion at later time-points. We observed a rapid formation of the glial scar already at 7 dpi (Fig. 5D). Analyzing the expression of the two astrocytic markers, Thbs4 and GFAP, as a percentage of the glial scar region-of-interest (ROI), we observed different dynamics and localization. GFAP expression increased rapidly after 7 days within the glial scar ROI, whereas Thbs4 was upregulated at 15 dpi (Fig. 5E). This delay suggested that the glial scar harbors two different astrocytic sub-populations: GFAP-only or GFAP/Thbs4. To analyze the spatial location of GFAP and Thbs4 markers within the Nestin border, we measured the fluorescence intensity profile of damaged area at 30 dpi. GFAP was found in both the scar and core areas, whereas Thbs4 fluorescence was found mostly at the borders of the glial scar (Fig. 5F-G). Analysis and dynamics of Thbs4-positive astrocyte migration was further performed in the corpus callosum (CC), striatum (Str), cortex (Ctx) and olfactory bulb (OB) (Fig. S5A). We observed a linear increase of Thbs4-positive astrocytes from 7 to 60 dpi, both in the Ctx and Str (Fig. S5B). Migration occurred mainly through the corpus callosum; among the total GFAP-positive astrocytes, 36.5% were also positive for Thbs4, suggesting that more than one third of the astrocytes in the glial scar derived from the SVZ (Fig. S5C). Likewise, the number of DCX-positive cells dramatically decreased 15 dpi in all OB layer (Fig. S5D-F) together with a significant decrease of BrdU-positive cells (Fig. S5G) DCX/BrdU- positive neuroblasts in the RMS (Fig. S5H), suggesting that ischemia induced a change in the neuroblasts ectopic migratory pathway, depriving the OB layers of the SVZ newborn neurons.

Thbs4-positive astrocytes modulate extracellular matrix homeostasis at the glial scar

To study the role of Thbs4-positive astrocytes in the glial scar, we analyzed the HA, the main compound of the brain extracellular matrix (ECM), using the hyaluronic binding protein (HABP) as a marker. Upon ischemic damage, local astrocytes (GFAP+/Thbs4-) react and change their morphology to a fibrotic state, producing high-molecular weight HA (HMW-HA) to form the glial scar and isolate the damaged area (Preston and Sherman, 2011). We then analyzed HA deposition in the corpus callosum and the infarcted areas after MCAO. HABP immunofluorescence (Fig. 6A) and image analysis evidenced HA accumulation in the infarcted areas. Skeleton analysis revealed progressively longer HA cable-like structures at the glial scar during infarct evolution (Fig. 6B). Fractal dimension analysis, which informs on the interconnectivity of the extracellular matrix (Soria et al., 2020), confirmed HA accumulation and progressively increased matrix complexity in infarcted areas but not in corpus callosum (Fig. 6C), suggesting that white matter glia react differently to the damage.

The presence of the Thbs4-positive astrocytes in the ischemic scar proximal to HA (Fig. 6D-E) prompted us to investigate if this population contributed to ECM production and, hence, to the scar formation. Since HA is produced exclusively at the cell membrane (Sherman et al., 2015; Zimmermann and Dours-Zimmermann, 2008), we analyzed HA labelling within 1 µm of the Thbs4-positive cell membrane in high-resolution confocal images (Fig. 6F). Image analysis showed a dramatic increase in HABP area at Thbs4-positive astrocyte-cell membranes after MCAO (Fig. 6G), suggesting a role of Thbs4-positive astrocytes in HA formation at the glial scar.

To study the potential role of Thbs4-positive astrocytes in HA removal, we quantified intracellular HABP spots in Thbs4-positive astrocytes at the glial scar. Although HMW-HA cleavage is an extracellular process, HA fragments can be internalized for degradation by lysosomal hyaluronidases (Preston and Sherman, 2011; Zimmermann and Dours-Zimmermann, 2008). Intracellular HABP spots were analyzed in the Thbs4-positive astrocytes and in local astrocytes GFAP-positive/Thbs4-negative) (Fig. S6A). Thirty days after MCAO, Thbs4-positive astrocytes showed more intracellular HABP than local astrocytes in the infarcted cortex (Fig. S6B). However, the number of HA spots internalized was

higher in local astrocytes compared with Thbs4 astrocytes (Fig. S6C), suggesting that Thbs4-positive cells internalize HA in fewer vesicles. To confirm that astrocytes were degrading HA, we performed an immunofluorescence analysis of CD44 (Fig. S6D). CD44 is a transmembrane glycoprotein receptor whose main function is HA degradation and ECM remodeling (Dzwonek and Wilczynski, 2015). We showed that Thbs4-positive astrocytes highly expressed CD44 receptor and their colocalization was around 80% of the total Thbs4-positive astrocytes in the corpus callosum 30 dpi (Fig. S6E). These results suggest that Thbs4- positive astrocytes participate in both the formation and degradation of the extracellular matrix at the glial scar.

To confirm these results in a more versatile preparation, we performed rat *in vitro* cultures from SVZ neural stem cells. Oxygen and glucose deprivation (OGD) protocol was conducted as an ischemia model and cells were fixed 7 days after OGD (Fig. S7A). HA was analysed by HABP immunofluorescence (Fig. S7B) inside and outside the Thbs4-positive cells (Fig. S7C). Thbs4-positive cells display increased intracellular HA after OGD (Fig. S7D), whereas HA decreased in the extracellular space (Fig. S7E). However, this phenomenon was reversed after adding hyaluronidases in the extracellular space (Fig. S7F-G), suggesting Thbs4-positive cells from SVZ homogenates can internalize or synthesize HA depending on the external stimuli. HA was also measured in Iba1-positive cell cultures where we observed a reduced internalization compare to Thbs4-positive cells (Fig. S7H). Finally, metalloproteinases activity was also increased in Thbs4 cultures after OGD (Fig. S7I). All these results together suggest Thbs4-positive cells can internalize HA after ischemic conditions but also synthetize it when ECM is degraded.

Hyaluronan accumulation is sufficient but not exclusive for the recruitment of Thbs4-positive astrocytes

Since Thbs4-positive astrocytes migrate to the glial scar but not to the ischemic core, we hypothesize that HA, the main component of the ischemic scar, may be the trigger signal for Thbs4-positive astrocyte recruitment. To test this hypothesis, we simulated the ECM accumulation occurring at the scar

by overexpressing the Hyaluronan synthase 2 (HAS2) from the naked mole rat (*Heterocephalus glaber*), which produces HA of very high molecular weight (Tian et al., 2013). We used a viral vector (AAV2/9-CAG-HAS2-3xFlag) with a FLAG tag to visualize transduced cells after intracerebral inoculation in the striatum and checked HA accumulation in FLAG-positive areas by HABP staining (Fig. 7A). We overexpressed HAS2 (or GFP as control) unilaterally, and in a subset of animals were MCAO was performed, the AAV-HAS2 was injected contralateral to the infarct, to compare Thbs4-positive astrocytes recruitment by both signals (Fig. 7B). FLAG-positive cells were quantified as a surrogate marker of viral infection for both control and MCAO groups (Fig. 7C). GFP control group did not increase HA production *per se* (Fig. 7D). However, HA overexpression was observed in HAS2 groups (both control and MCAO group) by HABP immunofluorescence (Fig. 7E-F).

HA accumulation was sufficient to recruit the Thbs4-positive astrocytes from the ipsilateral SVZ 45 days after the inoculation of AAV-HAS2 (Fig. 7G), with a time window similar to that observed after MCAO. Interestingly, when we produced the lesion by MCAO and the viral overexpression of HAS2 in the contralateral hemisphere, we observed that Thbs4-positive astrocytes preferentially migrated to the ischemic glial scar (Fig. 7G). The migration of Thbs4-positive astrocytes to the ischemic damage was observed even though HA overexpression showed no changes in both contralateral (HAS2 infected) and ipsilateral hemisphere (infarcted area) (Fig. 7H). These results suggest that accumulation of HMW-HA *per se* is sufficient to activate and recruit the Thbs4-positive astrocytes from the SVZ, but the preferential migration to the ischemic scar indicates that brain ischemia generates a more powerful biochemical signal that contributes to the SVZ activation and the recruitment of newborn astrocytes.

Ischemia-induced gliogenesis at the SVZ correlates with local hyaluronan degradation

It is known that the niche microenvironment has a particular ECM composition (Kjell et al., 2020) and that niche stiffness plays an important role in the proliferation and differentiation of progenitors cells (Long and Huttner, 2019; Segel et al., 2019). Having observed the close association between Thbs4-positive astrocytes and the ECM at the glial scar, we decided to study the Thbs4/HA tandem in the SVZ

after MCAO (Fig. 8A). We did not observe changes in the HA area in the whole SVZ but a decrease 7 and 15 dpi in the dorsal SVZ (Fig. 8B-D). Skeleton analysis showed fragmentation of HA only in the dorsal SVZ at 7 and 15 dpi (Fig. 8E-G), i.e., earlier than the migration of these newborn astrocytes towards the lesion.

We next analyzed different genes related to HA degradation (*Hyase 1, 2* and *3*) and synthesis (*HAS 1 and HAS 2*). *Thbs4* and hypoxia-inducible factor 1-alpha (*Hif1a*) genes, which are known to be increased in the SVZ after brain ischemia (Benito-Muñoz et al., 2016; Liu et al., 2007), were also analyzed as controls. Fresh tissue from SVZ was extracted from sham, 15 and 30 dpi mice (Fig. 8H). We observed increased expression of all Hyases at 15 dpi and slightly decreased 30 dpi, whereas synthases (HAS) gradually increased from 15 to 30 dpi (Fig. 8I). We also observed an increase of Thbs4 and Hif1a 15 and 30 dpi (Fig. 8I). These results suggest that HA degradation in the SVZ correlates with the Thbs4 response to ischemia.

DISCUSSION

The effects of brain insult on adult neurogenesis have been extensively discussed, both in animal models and humans. However, whether these can activate the generation of newborn astrocytes from the neurogenic niches is still under debate. Neural stem cells in the adult brain represent a reminiscence of the embryonic radial glia. While some researchers propose that exhaustion of neurogenesis in the adult brain is the consequence of astrogliogenesis (Encinas et al., 2011), others define astrogliogenesis as a part of a neurorestorative program from the neurogenic niches (Bonzano et al., 2018; Sohn et al., 2015). Nevertheless, direct and clear evidence of the generation of newborn astrocytes from the SVZ or the SGZ has not been presented so far, nor has the role that newborn astrocytes may have in ageing and pathophysiological conditions. Here, we confirm that a strong and acute damage-associated stimulus in the brain, such as an ischemic infarct, prompts astrogliogenesis in the SVZ. We also demonstrate that these astrocytes, which are positive for Thbs4, migrate to the glial scar and modulate it, being capable of synthesis and degradation of hyaluronan, a main component of the ECM at the scar.

Our results are in agreement with previous observations, where cortical injury initiated by photothrombotic/ischemia can initiate a massive Thbs4-positive astrocyte production from the SVZ that is modulated by Notch activation (Benner et al., 2013). In this work, the authors suggested a clear involvement of the Thbs4-positive astrocytes in ischemic scar modulation. In fact, the homozygotic ablation of the Thbs4 gene resulted in abnormal glial scar formation and increased microvascular haemorrhage after brain ischemia. Our results also showed that the adult neurogenic niche at the SVZ responds early after the ischemic stroke, degrading local hyaluronan plausibly to modify niche stiffness and allow NSCs proliferation and differentiation. NSC labelling by *in vivo* postnatal electroporation allowed us to provide proof of the origin and migration of newborn Thbs4-positive astrocytes from the SVZ to the ischemic scar in response to the pathological process. It is interesting to note that Thbs4 is present in the newborn astrocytes that arrive at the scar, whereas local reactive astrocytes at the damaged area express GFAP only. It is plausible that the SVZ-derived newborn astrocytes express Thbs4 to be able to migrate to the ischemic area since Thbs4 deletion has been shown to be detrimental to the migration of SVZ-derived cells along the RMS (Girard et al., 2014).

It is interesting to notice that despite the local, "GFAP-only", reactive astrocytes at the scar are capable of forming the required ECM (Cregg et al., 2014; Wanner et al., 2013), we show that Thbs4-positive (Thbs4/GFAP) astrocytes are recruited from the SVZ to participate in scar formation likewise. It should be noted that contrary to the local reactive astrocytes, which are hastily generated and are located both at the center and border of the lesion, the newborn astrocytes recruited from the SVZ arrive later to the injury. We demonstrate that these Thbs4-positive astrocytes migrate all the way from the SVZ to the lesion and stop at the lesion border (defined precisely by Nestin staining), establishing residence at the scar but not beyond. The molecular signals that trigger gliogenesis at the SVZ and recruit newborn astrocytes to the lesion are still unclear. We have previously shown that adenosine, a byproduct of ATP hydrolysis, is a strong candidate, given that stimulates astrogliogenesis through A1 receptors after OGD *in vitro* and ischemia *in vivo* (Benito-Muñoz et al., 2016). Here, we have shown that viral-mediated overproduction of the principal component of the glial scar, HA, is sufficient to activate the generation and migration of the Thbs4-positive astrocytes from the SVZ. However, our data also show that the

ischemic infarct, with all its proinflammatory (cytokines, chemokines) and proteolytic (MMPs, ROS) signals (Jayaraj et al., 2019), constitute a stronger attractor than the ECM *per se*.

Based on our observations of both HA production and internalization by these cells *in vivo* in the ischemic region and *in vitro* after OGD, we propose a role of Thbs4-positive astrocytes in the modulation, and perhaps maintenance, of the ECM at the scar. It is possible that ECM degradation at the scar is also performed by professional macrophages such as microglia, which are known to be recruited to the scar (Fawcett and Asher, 1999) and have been shown to degrade ECM by phagocytosis (Nguyen et al., 2020; Soria et al., 2020). Understanding which cells in the scar environment participate in its modulation, and specifically in its degradation, bears highly therapeutic value for regeneration (Silver and Miller, 2004). Here, we shed light on the unknown role of SVZ-derived astrocytes activated by the brain ischemic insult and propose them as critical players for tissue regeneration after brain ischemia.

ACKNOWLEDGEMENTS

The authors thank Juan Carlos Chara, Zara Martínez-Paez, and Laura Escobar for their invaluable technical support. We thank Abraham Martín, Mónica Benito-Muñoz and Sol Beccari for training in MCAO in mice. We also thank Vera Gorbunova (University of Rochester, USA) for providing the cDNA of HAS2 from the naked mole rat. We thank Marie-Laure Thiolat and Dr. Nathalie Dutheil for AAV production. F.C. acknowledges funding from BIOEF (BIO21/COV/012), Eukampus, Plan Complementario en Salud (PRTR-C17.I1) and the Basque Government. F.N.S. was funded by the Spanish Research Agency (IJCI-2017-32114, PID2020-115896RJ-I00 and RYC2021-032602-I co-funded by NextGeneration EU/PRTR). C.M. acknowledges funding from the Basque Government (IT1203-19) and CIBERNED. M.A. was supported by a PhD fellowship from the Basque Government.

AUTHOR CONTRIBUTIONS

M.A. conducted experiments and collected and analyzed data. M.C.T. and H.C. provided the Ai14-Rosa26-CAG-tdTomato$^{flx/flx}$ mice and technical input for electroporation. B.D. provided the AAV-HAS2 and conceived the idea of glial scar simulation. F.C., F.N.S. and C.M. secured funding. C.M. provided infrastructural support and scientific feedback. F.C. and F.N.S. conceived and supervised the study. F.P.C. supervised the study. M.A. and F.N.S. prepared the figures. M.A., F.N.S. and F.C. wrote the paper, with input from all authors.

METHODS

Animals

Male and female wild-type C57BL6/J mice and Ai14-Rosa26-CAG-tdTomato$^{flx/flx}$ transgenic mice bred at the animal facility of UPV/EHU were used for *in vivo* experiments. Sprague Dawley rat pups from P4 to P7 were used for *in vitro* experiments. All animals for *in vitro* and *in vivo* studies were handled in accordance with the European Communities Council Directive (2010/63/EU). All possible efforts were made to minimize animal suffering and the number of animals used. Animals were maintained under standard laboratory conditions with food and water *ad libitum*.

Transient MCAO

Brain ischemia was induced in 3-4-month old C57BL/6 mice (approximately 25 g) by occluding 60 minutes of the lenticulo-striate arteries with a 10 mm length of silicone-coated 6-0 monofilament nylon suture (602223PK10, Doccol Corporation) using a modification of the protocol described by (Gelderblom et al., 2009). Arteries occlusion generated a specific lesion in the cortex and striatum that was evaluated at different times after the MCAO (7, 15, 30 or 60 days after occlusion). Ischemic damage was evaluated in the ipsi-lateral hemisphere by Cresyl violet staining, nestin immunofluoresce or hyaluronan staining. Sham animals, in which arteries were visualized but not disturbed, were used as an experimental control. Both experimental groups, sham and ischemic, were anesthetized with a mix of isofluorane and oxygen (induction of anesthesia with 4% isofluorane and maintenance for surgery at 1.5% isofluorane) and maintained under analgesia with buprenorphine 24 hours after ischemia (0.03 mg/Kg body weight i.p. every 12h). Animal wellness was evaluated daily, controlling the body weight and the motor deficit of the animal by means of neurological score and pole test. Motor deficit was assessed in each animal 1h after MCAO and later every 24h. Animals without neurological deficits were excluded from the study.

5-bromo-2'-deoxyuridine (BrdU) protocol

The total pool of proliferating cells was labelled with three injections of 50 mg/kg 5-bromo-2'-deoxyuridine (BrdU) the day before MCAO protocol. Animals were sacrificed the day after MCAO to analyse acute SVZ proliferation. Chronic BrdU protocol was performed for quiescent NSC identification (Codega et al., 2014). Briefly, 1% of BrdU was administered in the drinking water during 14 days. At day 15, BrdU was removed and animals were subjected to MCAO protocol. Mice were sacrificed and perfused at 3, 7, 15 and 30 days after MCAO, although only animals with a temporal window of 30 days between MCAO and perfusion were used for statistical analysis. Activated cells were labelled by i.p. injection of 50 mg/Kg 5-iodo-2′-deoxyuridine (IdU) 24 hours before euthanasia.

Electroporation

Ai14-Rosa26-CAG-tdTomato$^{flx/flx}$ transgenic mice and pCAGGS-CRE plasmid were kindly provided for Prof. Harold Cremer and Marie-Catherine Tiveron from Institut de Biologie du Développement de Marseille (IBDM). Postnatal electroporation was performed as described previously (Platel et al., 2019). Mice pups from P0-P2 were anesthetized by hypothermia. pCAGGS-CRE plasmid was used at a final concentration of 2.5 µg/ul and 2µl was injected in the lateral ventricle by expiratory pressure using a glass micropipette. Following injection, pup brains were placed between electrodes targeted the dorsal SVZ and subjected to five 95V electrical pulses (50 ms, 950 ms intervals). BTX ECM399 (Thermo Fisher Scientific) electroporator was used with 7 mm tweezer electrodes. Electroporated pups were reanimated at 37ºC before returning to the mother.

AAV vector production

AAV2/9-CAG-HAS2-3xFlag vector was produced by polyethylenimine (PEI) mediated triple transfection of low passage HEK-293 T/17 cells (ATCC; cat number CRL-11268). The respective AAV

expression plasmid expression plasmid pNMRHAS2_N1(provided by Dr Vera Gorbunova) was cotransfected with the adeno helper pAd Delta F6 plasmid (Penn Vector Core, cat # PL-F-PVADF6) and AAV Rep Cap pAAV2/9 plasmid (Penn Vector Core, cat # PL-TPV008). AAV vector was purified as previously described (Bourdenx et al., 2015). Cells are harvested 72 h post-transfection, resuspended in lysis buffer (150 mM NaCl, 50 mM Tris–HCl pH 8.5) and lysed by 3 freeze-thaw cycles (37°C/-80°C). The cell lysate is treated with 150 units/ml Benzonase (Sigma, St Louis, MO) for 1 h at 37°C, and the crude lysate is clarified by centrifugation. Vectors are purified by iodixanol step gradient centrifugation and concentrated and buffer-exchanged into Lactated Ringer's solution (Baxter, Deerfield, IL) using vivaspin20 100 kDa cut-off concentrator (Sartorius Stedim, Goettingen, Germany). Titrations were performed at the transcriptome core facility (Neurocentre Magendie, INSERM U862, Bordeaux, France). The genome-containing particle (gcp) titer was determined at a concentration of 1.10^{13} gcp/ml by quantitative real-time PCR using the Light Cycler 480 SYBR green master mix (Roche, cat # 04887352001) with primers specific for the AAV2 ITRs (fwd 50-GGAACCCCTAGTGATG GAGTT-3'; rev 50-CGGCCTCAGTGAGCGA-30) on a Light Cycler 480 instrument. The purity assessment of vector stocks was estimated by loading 10 µl of vector stock on 10 % SDS acrylamide gels; total proteins were visualized using the Krypton Infrared Protein Stain according to the manufacturer's instructions (Life Technologies).

In vivo AAV-HAS2 injections

Mice were anaesthetized with isofluorane and fixed to a stereotaxic frame connected with a gas mask. We injected 1µl of adeno-associated virus (AAV2/9) CAG-HAS2-3xFlag (1x10^13 gc/µl) in the contralateral striatum (AP: +1.0; ML: -1.8; DV: -3.2) to simulate scar tissue hyaluronan. After two weeks, the ischemic group was subjected to the MCAO model in the ipsilateral hemisphere and perfused 30 days later. Only slices with representative lesions in both hemispheres were used for image and statistical analysis.

Immunofluorescence

Mice were anaesthetized with an intraperitoneal injection of pentobarbital (100 mg/kg). Brain tissues were fixed by intracardial perfusion using 4% paraformaldehyde. Fixed brains were sliced at 40 µm of thickness using the Leica VT 1200S vibratome (Leica Microsystems) and subjected to immunofluorescence. For standard immunofluorescence protocol, tissue slices were permeabilized with 0.1% Triton and non-specific epitopes blocked with 1% Bovine Serum Albumin and 10% Donkey serum in PBS. Primary antibodies (Supplementary Table 1) were incubated at different concentrations (see Table 1 for specification) overnight at 4ºC and then washed three times with 0.1% Triton in PBS. Secondary conjugated antibodies were incubated for 1 h at room temperature. After three washes with 0.1% Triton in PBS, cells were stained for 10 min with DAPI and further washed with PBS. Finally, coverslips were mounted with Fluoromount (SouthernBiotech) and analyzed by fluorescence using the confocal microscope Leica TCS SP8. For hyaluronic acid labelling, endogenous biotins were pre-blocked using Streptavidin/Biotin blocking solution (Vector Labs, #SP-2002) following the manufacturer´s instructions and further blocked with PBS 1X 0.1% Saponine 1% BSA for one hour at room temperature. Primary antibodies and biotinylated Hyaluronic Acid Binding Protein (HABP, #385911 Millipore) were incubated for 72 hours at 4°C or 24 hours at room temperature. After three washes with PBS, 1X 0.1% Saponine, secondary antibody and DAPI diluted in the same blocking buffer were incubated for one hour at room temperature. Slices were mounted with Mowiol (Millipore #475904) in superfrost slides (Thermo Fisher Scientific) and #1.5 coverslips.

Imaging and image analysis

Confocal images were acquired in a Leica TCS SP8, 1.4 NA and 63X oil magnification. Widefield imaging was performed in a Zeiss AxioVision fluorescence microscope and a 3DHISTECH panoramic MIDI II digital slide scanner. Settings were adjusted for each individual experiment and kept for all conditions. Image processing was performed using ImageJ, CaseViewer and Hyugens (SVI, The Netherlands) software. For Thbs4, Nestin and DCX immunofluorescence, wholemount SVZ

preparations and AAV-HAS2 analysis, tile-scan was done using the navigator plug-in in the LasX software. For Nestin immunofluorescence, images were de-convoluted using the Hyugens software. For HABP analysis (both *in vitro* and *in vivo* analysis), an ImageJ macro was created in order to measure several parameters (HABP area and spots, inside and outside cell) with slight changes depending on the sample (monolayer or tissue).

Western blot

The SVZ was freshly dissected on ice and minced using a micro grinder. Total protein was extracted after tissue lysis with RIPA buffer (Thermo Fisher Scientific #89900) and Protease and Phosphatase Inhibitor Cocktail 100X (Thermo Fisher Scientific). Samples were lysed in ice for 10 minutes and sonicated using an Ultrasonic Processor (Hielscher Ultrasound Technology). Sonicated tissues were centrifuged at 1200 rpm for 10 min and 4°C to remove insoluble fragments. Protein concentration was measured by chemioluminescence using RC DC™ Protein Assay (Bio-Rad). Forty micrograms of protein samples were denatured in reducing loading buffer containing β-mercaptoethanol (M3148, Sigma) and 0.0002% bromophenol blue at 95°C for 5 minutes and separated in pre-casted 12% or 7.5% Tris-Glycine polyacrylamide gel using the Criterion cell system (Biorad). Electrophoresis was conducted at 80 V in a Tris-Glycine buffer (25 mM Tris, 192 mM glycine, 0.1% SDS in dH2O, pH 8.3). After complete separation, proteins were transferred to a nitrocellulose membrane (Biorad) using Trans-Blot® TurboTM Transfer System (Bio-Rad). Nitrocellulose membranes were incubated in blocking solution (Tris-Buffer Solution (TBS), 0.1% Tween-20 and 5% BSA) for one hour at room temperature. Primary antibodies were incubated overnight at 4°C. Horseradish peroxidase-conjugated secondary antibodies were incubated in blocking buffer for one hour at room temperature. Immunodetection was performed by electrochemical luminescence in a Chemidoc MP (Biorad) and the intensity of the bands was quantified using ImageLab (Bio-Rad) software corrected by Gaussian curves.

qRT-PCR

Fresh SVZ tissue from ipsilateral hemisphere was isolated as previously described from sham, 15 and 30 days after MCAO animals to analyse the expression of several genes (Supplementary Table 2). RNA was extracted from the tissue after mechanical trituration following the manufacturer´s protocol (NZYTECH Total RNA Isolation kit protocol (NZYTECH, MB13402). RNA concentration was measured by spectrophotometry using the Nanodrop 2000c spectrophotometer (Thermo-Scientific, USA). Real time polymerase chain reaction (RT-PCR) from 10 ng of RNA was performed using the One-step NZYTECH RT-qPCR Green kit according to manufacturer´s protocol (NZYTECH, MB34302). RT-PCR was normalized using the housekeeping genes hypoxanthine phosphoribosyl-transferase 1 (HPRT1, Qiagen QuantiTect Primer Assay, Barcelona, Spain). Specificity of each amplification was confirmed by melting curve analysis. PCR reactions were performed in a CFX96 Detection System (BioRad, Madrid, Spain). Semi-quantification was performed using the 2-ΔΔCt algorithm. Unsupervised hierarchical distance matrix and distance matrix map was developed using Orange3 software (Python v3.0).

Statistical analysis

Statistical analysis was done using GraphPad Prism software (version 8.0; GraphPad software). Data are presented as mean ± SEM unless specified otherwise. Statistical analysis was performed using unpaired Student´s t-test for independent conditions and paired Student´s t-test for dependent conditions. In addition, one-way and two-way ANOVA were also performed to compare more than 2 groups among them. Tukey and Dunnett post-hoc tests were used. For HABP skeleton analysis, Kruskal-Wallis analysis was performed to compare cumulative frequency curves in more than 2 groups. *P* value was considered significant at $p < 0.05$. Sample number (*n*), *p* values and statistical test are indicated in figure legends.

REFERENCES

Adams KL, Gallo V. 2018. The diversity and disparity of the glial scar. *Nat Neurosci* **21**:9–15. doi:10.1038/s41593-017-0033-9

Anderson MA, Burda JE, Ren Y, Ao Y, O'Shea TM, Kawaguchi R, Coppola G, Khakh BS, Deming TJ, Sofroniew MV. 2016. Astrocyte scar formation aids central nervous system axon regeneration. *Nature* **532**:195–200. doi:10.1038/nature17623

Arvidsson A, Collin T, Kirik D, Kokaia Z, Lindvall O. 2002. Neuronal replacement from endogenous precursors in the adult brain after stroke. *Nat Med* **8**:963–970. doi:10.1038/nm747

Benito-Muñoz M, Matute C, Cavaliere F. 2016. Adenosine A1 receptor inhibits postnatal neurogenesis and sustains astrogliogenesis from the subventricular zone. *Glia* **64**:1465–1478. doi:10.1002/glia.23010

Benner EJ, Luciano D, Jo R, Abdi K, Paez-Gonzalez P, Sheng H, Warner DS, Liu C, Eroglu C, Kuo CT. 2013. Protective astrogenesis from the SVZ niche after injury is controlled by Notch modulator Thbs4. *Nature* **497**:369–373. doi:10.1038/nature12069

Bond AM, Ming G-L, Song H. 2015. Adult Mammalian Neural Stem Cells and Neurogenesis: Five Decades Later. *Cell Stem Cell* **17**:385–395. doi:10.1016/j.stem.2015.09.003

Bonzano S, Crisci I, Podlesny-Drabiniok A, Rolando C, Krezel W, Studer M, De Marchis S. 2018. Neuron-Astroglia Cell Fate Decision in the Adult Mouse Hippocampal Neurogenic Niche Is Cell-Intrinsically Controlled by COUP-TFI In Vivo. *Cell Rep* **24**:329–341. doi:10.1016/j.celrep.2018.06.044

Bourdenx M, Dovero S, Engeln M, Bido S, Bastide MF, Dutheil N, Vollenweider I, Baud L, Piron C, Grouthier V, Boraud T, Porras G, Li Q, Baekelandt V, Scheller D, Michel A, Fernagut P-O, Georges F, Courtine G, Bezard E, Dehay B. 2015. Lack of additive role of ageing in nigrostriatal neurodegeneration triggered by α-synuclein overexpression. *Acta Neuropathol Commun* **3**:46. doi:10.1186/s40478-015-0222-2

Bush TG, Puvanachandra N, Horner CH, Polito A, Ostenfeld T, Svendsen CN, Mucke L, Johnson MH, Sofroniew MV. 1999. Leukocyte infiltration, neuronal degeneration, and neurite outgrowth after ablation of scar-forming, reactive astrocytes in adult transgenic mice. *Neuron* **23**:297–308. doi:10.1016/s0896-6273(00)80781-3

Cavaliere F, Dinkel K, Reymann K. 2006. The subventricular zone releases factors which can be protective in oxygen/glucose deprivation-induced cortical damage: an organotypic study. *Exp Neurol* **201**:66–74. doi:10.1016/j.expneurol.2006.03.020

Ceanga M, Dahab M, Witte OW, Keiner S. 2021. Adult Neurogenesis and Stroke: A Tale of Two Neurogenic Niches. *Frontiers in Neuroscience* **15**.

Chaker Z, Codega P, Doetsch F. 2016. A mosaic world: puzzles revealed by adult neural stem cell heterogeneity. *WIREs Developmental Biology* **5**:640–658. doi:10.1002/wdev.248

Codega P, Silva-Vargas V, Paul A, Maldonado-Soto AR, DeLeo AM, Pastrana E, Doetsch F. 2014. Prospective Identification and Purification of Quiescent Adult Neural Stem Cells from Their In Vivo Niche. *Neuron* **82**:545–559. doi:10.1016/j.neuron.2014.02.039

Cregg JM, DePaul MA, Filous AR, Lang BT, Tran A, Silver J. 2014. Functional regeneration beyond the glial scar. *Exp Neurol* **253**:197–207. doi:10.1016/j.expneurol.2013.12.024

Doetsch F, Caillé I, Lim DA, García-Verdugo JM, Alvarez-Buylla A. 1999. Subventricular zone astrocytes are neural stem cells in the adult mammalian brain. *Cell* **97**:703–716. doi:10.1016/s0092-8674(00)80783-7

Dzwonek J, Wilczynski GM. 2015. CD44: molecular interactions, signaling and functions in the nervous system. *Front Cell Neurosci* **9**:175. doi:10.3389/fncel.2015.00175

Encinas JM, Michurina TV, Peunova N, Park J-H, Tordo J, Peterson DA, Fishell G, Koulakov A, Enikolopov G. 2011. Division-coupled astrocytic differentiation and age-related depletion of neural stem cells in the adult hippocampus. *Cell Stem Cell* **8**:566–579. doi:10.1016/j.stem.2011.03.010

Faulkner JR, Herrmann JE, Woo MJ, Tansey KE, Doan NB, Sofroniew MV. 2004. Reactive astrocytes protect tissue and preserve function after spinal cord injury. *J Neurosci* **24**:2143–2155. doi:10.1523/JNEUROSCI.3547-03.2004

Fawcett JW. 2015. Chapter 10 - The extracellular matrix in plasticity and regeneration after CNS injury and neurodegenerative disease In: Dancause N, Nadeau S, Rossignol S, editors. Progress in Brain Research, Sensorimotor Rehabilitation. Elsevier. pp. 213–226. doi:10.1016/bs.pbr.2015.02.001

Fawcett JW, Asher RA. 1999. The glial scar and central nervous system repair. *Brain Res Bull* **49**:377–391. doi:10.1016/s0361-9230(99)00072-6

Frisén J, Johansson CB, Török C, Risling M, Lendahl U. 1995. Rapid, widespread, and longlasting induction of nestin contributes to the generation of glial scar tissue after CNS injury. *Journal of Cell Biology* **131**:453–464. doi:10.1083/jcb.131.2.453

Gelderblom M, Leypoldt F, Steinbach K, Behrens D, Choe C-U, Siler DA, Arumugam TV, Orthey E, Gerloff C, Tolosa E, Magnus T. 2009. Temporal and spatial dynamics of cerebral immune cell accumulation in stroke. *Stroke* **40**:1849–1857. doi:10.1161/STROKEAHA.108.534503

Girard F, Eichenberger S, Celio MR. 2014. Thrombospondin 4 deficiency in mouse impairs neuronal migration in the early postnatal and adult brain. *Molecular and Cellular Neuroscience* **61**:176–186. doi:10.1016/j.mcn.2014.06.010

Jayaraj RL, Azimullah S, Beiram R, Jalal FY, Rosenberg GA. 2019. Neuroinflammation: friend and foe for ischemic stroke. *J Neuroinflammation* **16**:142. doi:10.1186/s12974-019-1516-2

Kjell J, Fischer-Sternjak J, Thompson AJ, Friess C, Sticco MJ, Salinas F, Cox J, Martinelli DC, Ninkovic J, Franze K, Schiller HB, Götz M. 2020. Defining the Adult Neural Stem Cell Niche Proteome Identifies Key Regulators of Adult Neurogenesis. *Cell Stem Cell* **26**:277-293.e8. doi:10/ghcp5v

Kralic JE, Ledergerber DA, Fritschy J-M. 2005. Disruption of the neurogenic potential of the dentate gyrus in a mouse model of temporal lobe epilepsy with focal seizures. *European Journal of Neuroscience* **22**:1916–1927. doi:10.1111/j.1460-9568.2005.04386.x

Lau LW, Cua R, Keough MB, Haylock-Jacobs S, Yong VW. 2013. Pathophysiology of the brain extracellular matrix: a new target for remyelination. *Nat Rev Neurosci* **14**:722–729. doi:10/f5b6w9

Laug D, Huang T-W, Huerta NAB, Huang AY-S, Sardar D, Ortiz-Guzman J, Carlson JC, Arenkiel BR, Kuo CT, Mohila CA, Glasgow SM, Lee HK, Deneen B. 2019. Nuclear factor I-A regulates diverse reactive astrocyte responses after CNS injury. *J Clin Invest* **129**:4408–4418. doi:10.1172/JCI127492

Li L, Harms KM, Ventura PB, Lagace DC, Eisch AJ, Cunningham LA. 2010. Focal cerebral ischemia induces a multilineage cytogenic response from adult subventricular zone that is predominantly gliogenic. *Glia* **58**:1610–1619. doi:10.1002/glia.21033

Liu XS, Zhang ZG, Zhang RL, Gregg SR, Meng H, Chopp M. 2007. Comparison of in vivo and in vitro gene expression profiles in subventricular zone neural progenitor cells from the adult mouse after middle cerebral artery occlusion. *Neuroscience* **146**:1053–1061. doi:10.1016/j.neuroscience.2007.02.056

Long KR, Huttner WB. 2019. How the extracellular matrix shapes neural development. *Open Biol* **9**:180216. doi:10/ghn8hs

Luskin MB. 1993. Restricted proliferation and migration of postnatally generated neurons derived from the forebrain subventricular zone. *Neuron* **11**:173–189. doi:10.1016/0896-6273(93)90281-u

Nguyen PT, Dorman LC, Pan S, Vainchtein ID, Han RT, Nakao-Inoue H, Taloma SE, Barron JJ, Molofsky AB, Kheirbek MA, Molofsky AV. 2020. Microglial Remodeling of the Extracellular Matrix Promotes Synapse Plasticity. *Cell* **182**:388-403.e15. doi:10/gg5cj3

Platel J-C, Angelova A, Bugeon S, Wallace J, Ganay T, Chudotvorova I, Deloulme J-C, Béclin C, Tiveron M-C, Coré N, Murthy VN, Cremer H. 2019. Neuronal integration in the adult mouse olfactory bulb is a non-selective addition process. *eLife* **8**:e44830. doi:10.7554/eLife.44830

Pous L, Deshpande SS, Nath S, Mezey S, Malik SC, Schildge S, Bohrer C, Topp K, Pfeifer D, Fernández-Klett F, Doostkam S, Galanakis DK, Taylor V, Akassoglou K, Schachtrup C. 2020. Fibrinogen induces neural stem cell differentiation into astrocytes in the subventricular zone via BMP signaling. *Nat Commun* **11**:630. doi:10.1038/s41467-020-14466-y

Preston M, Sherman LS. 2011. Neural Stem Cell Niches: Critical Roles for the Hyaluronan-Based Extracellular Matrix in Neural Stem Cell Proliferation and Differentiation. *Front Biosci (Schol Ed)* **3**:1165–1179.

Segel M, Neumann B, Hill MFE, Weber IP, Viscomi C, Zhao C, Young A, Agley CC, Thompson AJ, Gonzalez GA, Sharma A, Holmqvist S, Rowitch DH, Franze K, Franklin RJM, Chalut KJ. 2019. Niche stiffness underlies the ageing of central nervous system progenitor cells. *Nature* **573**:130–134. doi:10/gf6j83

Sherman LS, Matsumoto S, Su W, Srivastava T, Back SA. 2015. Hyaluronan Synthesis, Catabolism, and Signaling in Neurodegenerative Diseases. *International Journal of Cell Biology* **2015**:e368584. doi:10/gccgm9

Silver J, Miller JH. 2004. Regeneration beyond the glial scar. *Nat Rev Neurosci* **5**:146–156. doi:10.1038/nrn1326

Sohn J, Orosco L, Guo F, Chung S-H, Bannerman P, Mills Ko E, Zarbalis K, Deng W, Pleasure D. 2015. The subventricular zone continues to generate corpus callosum and rostral migratory stream astroglia in normal adult mice. *J Neurosci* **35**:3756–3763. doi:10.1523/JNEUROSCI.3454-14.2015

Soria FN, Paviolo C, Doudnikoff E, Arotcarena M-L, Lee A, Danné N, Mandal AK, Gosset P, Dehay B, Groc L, Cognet L, Bezard E. 2020. Synucleinopathy alters nanoscale organization and diffusion in the brain extracellular space through hyaluronan remodeling. *Nat Commun* **11**:3440. doi:10.1038/s41467-020-17328-9

Sundholm-Peters NL, Yang HKC, Goings GE, Walker AS, Szele FG. 2005. Subventricular Zone Neuroblasts Emigrate Toward Cortical Lesions. *Journal of Neuropathology & Experimental Neurology* **64**:1089–1100. doi:10.1097/01.jnen.0000190066.13312.8f

Tian X, Azpurua J, Hine C, Vaidya A, Myakishev-Rempel M, Ablaeva J, Mao Z, Nevo E, Gorbunova V, Seluanov A. 2013. High-molecular-mass hyaluronan mediates the cancer resistance of the naked mole rat. *Nature* **499**:346–349. doi:10/ghcp25

Wanner IB, Anderson MA, Song B, Levine J, Fernandez A, Gray-Thompson Z, Ao Y, Sofroniew MV. 2013. Glial Scar Borders Are Formed by Newly Proliferated, Elongated Astrocytes That Interact to Corral Inflammatory and Fibrotic Cells via STAT3-Dependent Mechanisms after Spinal Cord Injury. *J Neurosci* **33**:12870–12886. doi:10.1523/JNEUROSCI.2121-13.2013

Yamashita T, Ninomiya M, Hernández Acosta P, García-Verdugo JM, Sunabori T, Sakaguchi M, Adachi K, Kojima T, Hirota Y, Kawase T, Araki N, Abe K, Okano H, Sawamoto K. 2006. Subventricular zone-derived neuroblasts migrate and differentiate into mature neurons in the post-stroke adult striatum. *J Neurosci* **26**:6627–6636. doi:10.1523/JNEUROSCI.0149-06.2006

Young SZ, Taylor MM, Wu S, Ikeda-Matsuo Y, Kubera C, Bordey A. 2012. NKCC1 knockdown decreases neuron production through GABA(A)-regulated neural progenitor proliferation and delays dendrite development. *J Neurosci* **32**:13630–13638. doi:10.1523/JNEUROSCI.2864-12.2012

Zimmermann DR, Dours-Zimmermann MT. 2008. Extracellular matrix of the central nervous system: from neglect to challenge. *Histochem Cell Biol* **130**:635–653. doi:10.1007/s00418-008-0485-9

FIGURES

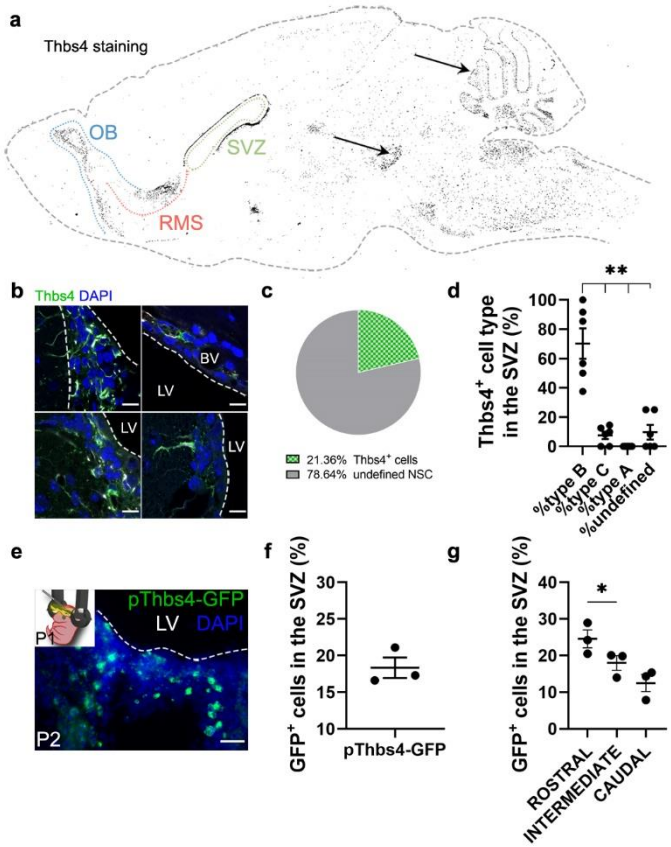

Figure 1 – Thbs4 labels type-B cells at the neurogenic niche in the SVZ. (a) Brain schematic drawing showing Thbs4 labelling throughout the mouse brain. Thbs4 was mainly found in the SVZ and RMS in the adult mouse telencephalon. Arrows point to unspecific Thbs4 staining in cerebellum and ventral tegmental area. (b) Thbs4 positive cells in the SVZ showed different morphologies. (c) Proportion of Thbs4-positive cells among the total cell population at the SVZ. (d) Classification of Thbs4-positive cells in the SVZ according to their NSC morphology. (e) Electroporation of pThbs4-GFP at P1 revealed Thbs4 expression in the post-natal dorsal SVZ. (f) Quantification of Thbs4-reporter expression showing the proportion of NSC expressing Thbs4 postnatally in the dorsal SVZ. (g) Thbs4-GFP reporter expression was higher expressed in the rostral SVZ. BV: Blood vessel; LV: Lateral ventricle. Scale bar = 10 µm (b) and 50 µm (e). Bars represent mean ± SEM. *$p<0.05$ and **$p<0.01$, Tukey post hoc test (after one-way ANOVA was significant at $p < 0.05$).

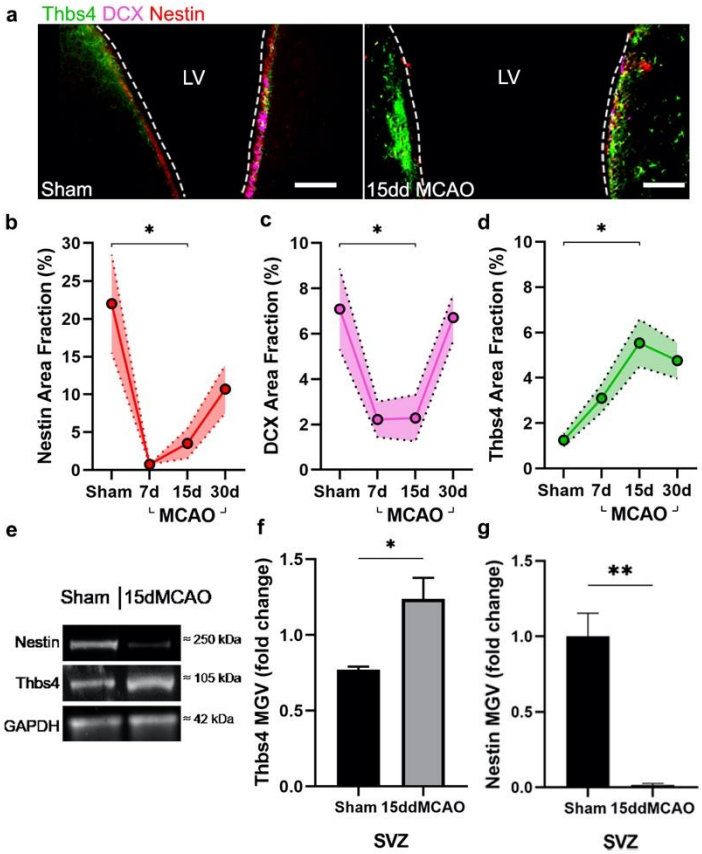

Figure 2 – Thbs4 increase in the SVZ after brain ischemia. (a) Representative images of Thbs4 (green), Nestin (red) and DCX (magenta) markers in physiological (left) and 15 days post-injury (dpi) SVZ (right). (b,c) Active proliferating NSCs and neuroblast decrease at 7 and 15 dpi in the SVZ, as shown by Nestin (b) and DCX (c) levels respectively. decreased 7 and 15 dpi in the SVZ. (c) DCX marker (neuroblasts) decreased 7 and 15 dpi in the SVZ. (d) Thbs4 expression increased in the SVZ after the ischemic insult over time. (e) Representative images of Nestin and Thbs4 protein in sham and 15 dpi SVZ by western blot. (f,g) Quantification of mean gray value (MGV) levels from (e), normalized to GAPDH, show Thbs4 (f) increase and Nestin decrease (g) in the 15 dpi SVZ. Scale bar = 100 µm in (a). n = 6 (b, c, d) and 3 (e, f, g) for each condition. Bars represent mean ± SEM. *$p < 0.05$ and **$p < 0.01$; two-tail Student´s t test (sham vs. 15ddMCAO) and Tukey post-hoc test (after one-way ANOVA was significant at $p < 0.05$). See also Supplementary Figures 1 and 2.

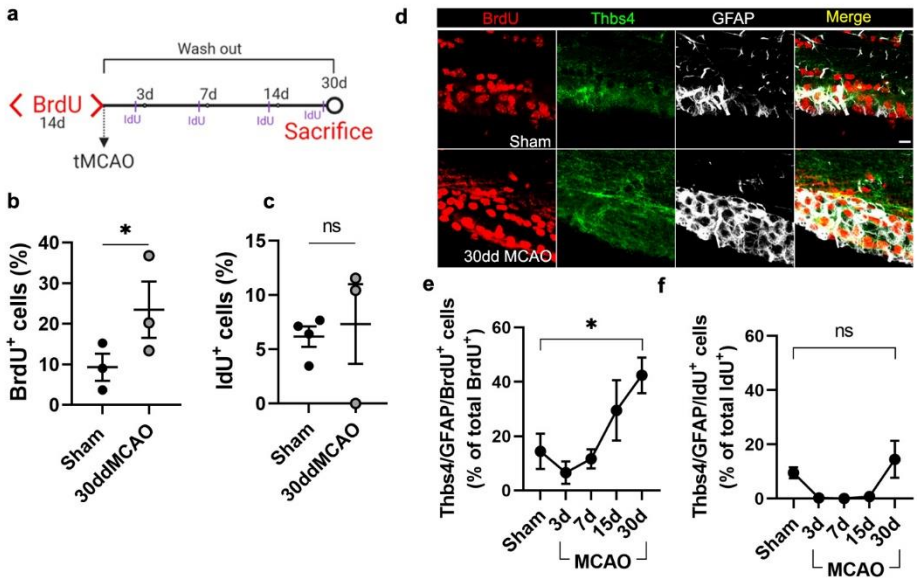

Figure 3 – Thbs4-positive cells derive from B-type NSC in the SVZ after brain ischemia. (a) Experimental design: chronic BrdU (1% in water) treatment was administered for two weeks. BrdU only persisted in B-type NSCs 30 days after treatment. Animals were injected three times with IdU (50 mg/kg) to label proliferating cells the day before euthanasia. (b,c) BrdU (b) and IdU (c) positive cells at the SVZ. Only BrdU cells are significantly increased at 30 dpi. (d) Representative confocal images of Thbs4, GFAP and BrdU levels in sham (top) and 30 dpi mice (bottom). (e,f) Thbs4/GFAP/BrdU positive cells (slow proliferative cells) increased in the SVZ 30 dpi (e), while no changes were found for Thbs4/GFAP/IdU positive cells (fast proliferative cells). Scale bar = 10 µm (d). n = 4 (sham) and 3 (MCAO). Bars represent mean ± SEM. *$p < 0.05$ by two-tail Student´s t-test (sham vs. 30dd MCAO). See also Supplementary Figure 3.

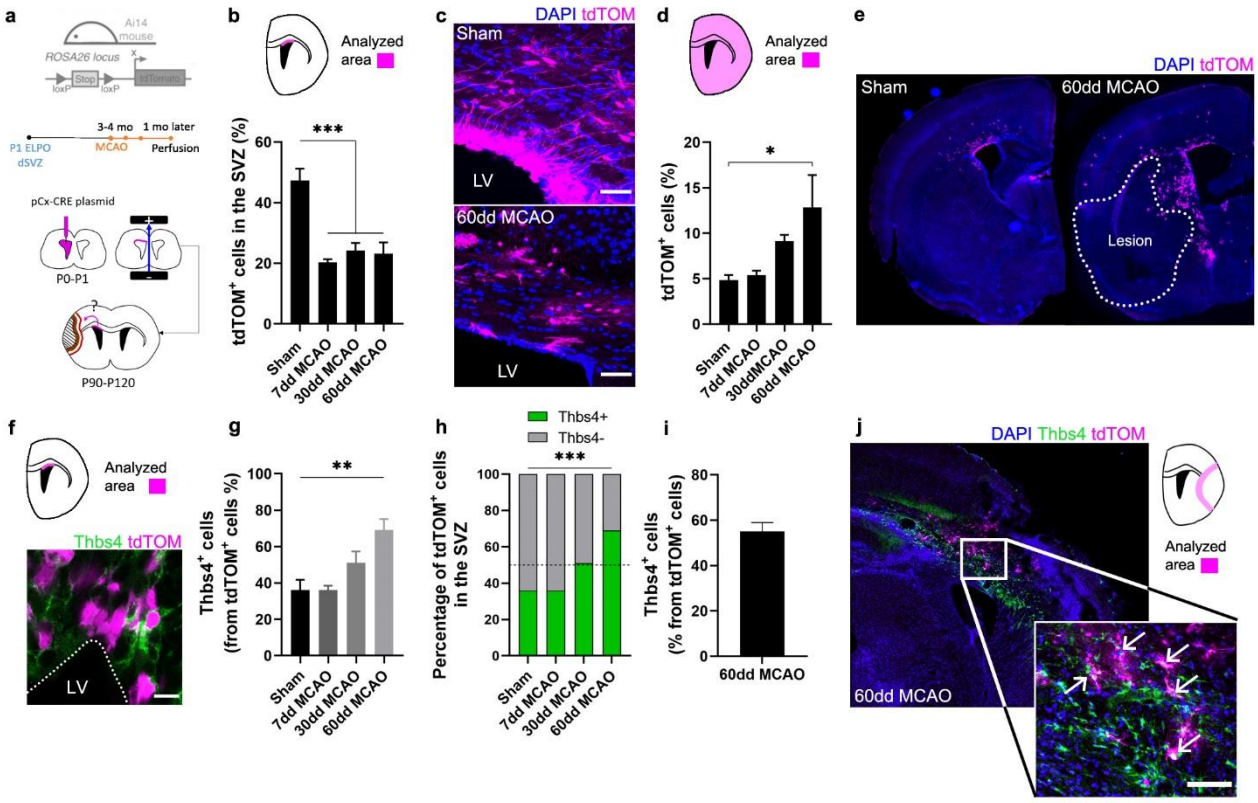

Figure 4 – Ischemia-induced Thbs4 astrocytes migrate from the SVZ to ischemic areas. (a) Experimental design: Ai14, ROSA26-CAG-tdTomato transgenic mice were electroporated in the dorsal SVZ at P1. pCAGGSx-CRE plasmid induced expression of tdTomato (tdTOM) in dorsal NSCs. MCAO was performed after 3-4 months in the same electroporated hemisphere. Mice were analyzed 7, 30 and 60 dpi. **(b)** Quantification of tdTOM-positive cells shows a decrease in the dorsal SVZ after brain ischemia. (c) Representative images of tdTOM positive cells in sham (top) and 60 dpi SVZ (bottom). (d) Quantification of tdTOM positive cells in the whole brain show incremental increase outside of the SVZ after brain ischemia. (e) Representative images of tdTOM expression in sham (left) and 60 dpi mice (right). (f) Representative image of Thbs4/tdTOM positive cells in the dorsal SVZ. (g) Quantification shows an increase of Thbs4/tdTOM-positive cells in the SVZ 30 and 60 dpi. (h) Proportion of Thbs4-positive cells in the tdTOM pool increases in the SVZ 30 and 60 dpi. (i) Around 50% of tdTOM-positive cells expressed Thbs4 in the infarcted tissue 60 dpi. (j) Representative image of Thbs4 and tdTOM expression near damaged area. Scale bar = 50 µm (c), 10 µm (f) and 100 µm (g). n = 6 animals per condition. Bars represent mean ± SEM. *$p < 0.05$, **$p < 0.01$ and ***$p < 0.001$ by Chi-square test (h) and Tukey posthoc test (after one-way ANOVA was significant at $p < 0.05$). See also Supplementary Figure 4.

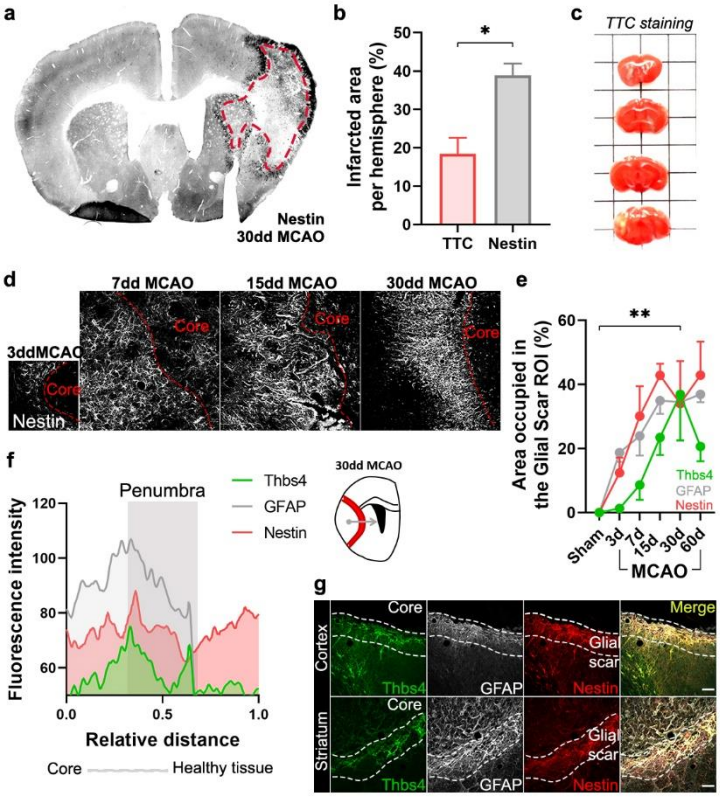

Figure 5 – Ischemia-induced Thbs4 astrocytes accumulate at the glial scar. (a) Glial scar could be observed at 30 dpi by Nestin immunofluorescence. (b) Classical TTC technique underestimated ischemic regions compared with Nestin immunofluorescence. (c) Representative images of TTC staining I infarcted brains. (d) Representative confocal images showing the time course of Nestin expression at 3, 7, 15 and 30 dpi. (e) Nestin glial scar was established by 15 dpi. Thbs4 astrocytes arrived at the glial scar later, by 30 dpi. (f) Fluorescence profile of Thbs4, GFAP and Nestin marker from core to penumbra areas shown Thbs4 was mainly located in the borders of the Nestin-positive glial scar. (g) Representative images of Thbs4 (green), GFAP (white) and Nestin (red) markers in sham (top) and 30 dpi mice (bottom). Scale bar = 50 µm (g). n = 3 animals per condition. Bars/lines represent mean ± SEM. *$p < 0.05$ and **$p < 0.01$ by two-tail Student´s t test (TTC vs. Nestin) and by Dunnett posthoc test (after two-way ANOVA was significant at $p < 0.05$). See also Supplementary Figure 5.

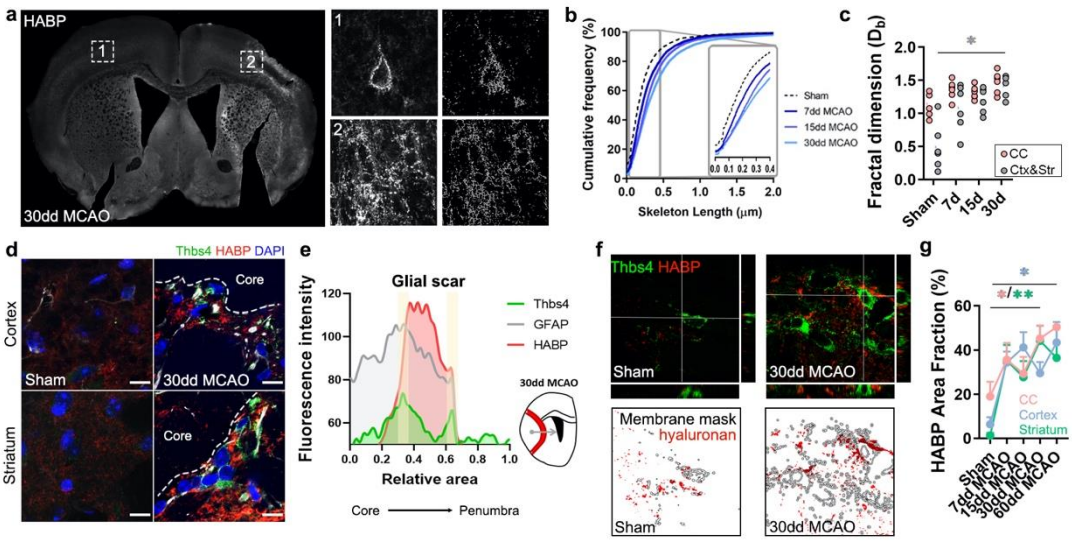

Figure 6 – Thbs4-positive astrocytes produce hyaluronan at the glial scar after MCAO. (a) Representative images of hyaluronic acid (HA) labelled with HABP in the contralateral (1) and ipsilateral hemisphere (2). Only perineuronal nets are clearly visible in the healthy tissue, while a dense interstitial matrix is observed in ischemic areas (b) Cumulative distribution of skeletonized HA signal in sham and infarcted regions of 7, 15 and 30 dpi mice ($p<0.0001$). (c) Quantification of fractal dimension showed increased extracellular matrix interconnectivity in the infarcted cortex and striatum (Ctx&Str) 30 dpi. (d) Representative confocal images of Thbs4 (green) and HABP (red) in the cortex and striatum of sham and 30 dpi mice. Notice the HA labelling on the surface of Thbs4-positive cells. (e) Fluorescence intensity profile of Thbs4, GFAP and HABP markers from lesion core to penumbra areas. Thbs4 expression was mainly restricted to the borders of the HA glial scar 30 dpi. ((f) Representative confocal images of Thbs4 and HABP markers in sham and 30 dpi mice (top). Examples of area occupied by HA (red) in the membrane mask of Thbs4 positive astrocytes in sham and 30 dpi mice (bottom), showing increased HA synthesis after MCAO. (g) Quantification of membrane-bound HA showed increased HA along Thbs4-positive membrane after brain ischemia (corpus callosum: pink; infarcted cortex: blue; infarcted striatum: green). Scale bar = 10 µm (e). n = 6 animals per condition. *$p < 0.05$ and ****$p < 0.0001$ by Krustal Wallis test and two-way ANOVA (significant at $p < 0.05$). See also Supplementary Figures 6 and 7.

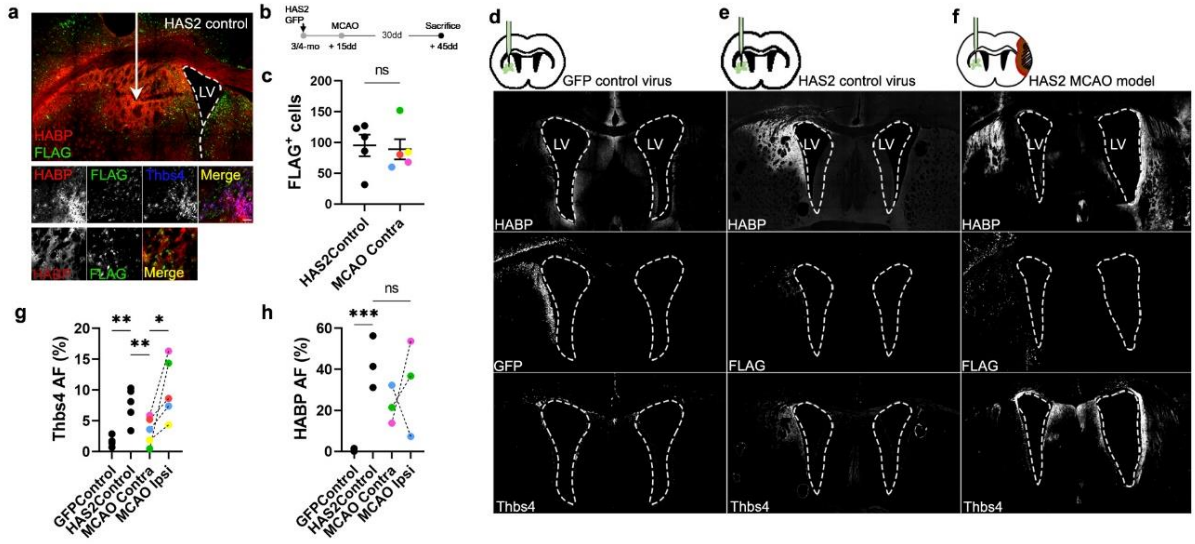

Figure 7 – Hyaluronan accumulation is sufficient but not exclusive to recruit Thbs4 astrocytes. (a) Representative images of HA accumulation caused by viral-mediated overexpression of HAS2 from naked mole rat. (b) Experimental design: HAS2 viral injections were performed 2 weeks before MCAO. Animals were sacrificed 30 days after MCAO. We used standard GFP virus as control. Two groups of HAS2 injected mice were performed. Only one of them was subjected to MCAO. (c) FLAG-positive cells (HAS2 virus tag) did not show changes in either HAS2 control (HAS2Control) or HAS2-MCAO group (MCAO contralateral hemisphere). (d,e,f) Representative images of HABP, GFP and Thbs4 markers in GFP control virus (d), HAS2 control virus (e) and HAS2 MCAO group (f). (g) Thbs4 expression increased after HAS2 viral-mediated overexpression. However, Thbs4 was upregulated in the ischemic hemisphere when MCAO was performed together with the HAS2 viral infection (MCAO ipsi). GFP control virus did not induce increase of Thbs4. (h) HABP was used as a control for HA accumulation. Thbs4 astrocytes in HAS2 MCAO group increased in the ischemic hemisphere even though HA accumulation was the same in both hemispheres (HAS2 and MCAO hemisphere), suggesting other ischemia-induced signals recruit Thbs4 astrocytes to infarcted areas. Scale bar = 100 µm (a). n = 6 animals per condition. *$p < 0.05$, **$p < 0.01$ and ***$p < 0.001$ by two-tail Student´s t test (HAS2Control vs. MCAO Contra) and Tukey posthoc test (after one-way ANOVA was significant at $p < 0.05$).

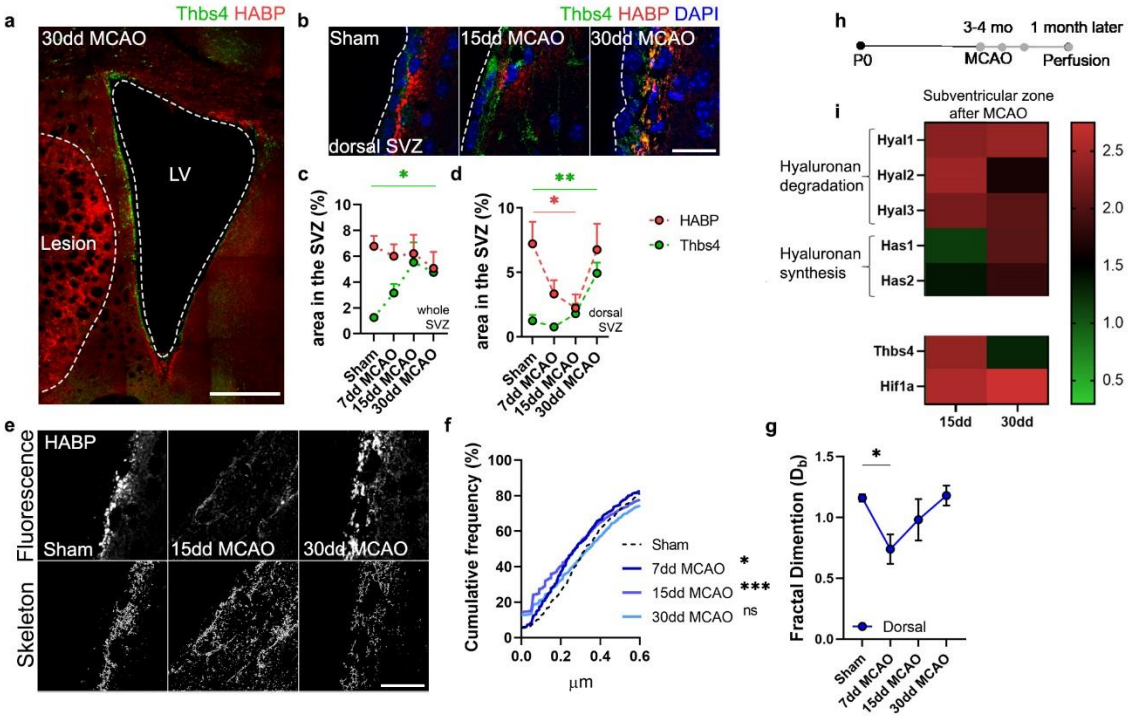

Figure 8 – HA degradation in the SVZ correlates with Thbs4 response to brain ischemia. (a) Representative image of Thbs4 and HA (HABP) markers in the SVZ 30 dpi. (b) Representative images of Thbs4 and HA in the sham and 15, 30 dpi SVZ. (c, d) HA signal did not change in the whole SVZ after MCAO (c) but decreased drastically in the dorsal SVZ (d). Thbs4 expression increased overall in the SVZ after MCAO (c), with a marked increase at 30 dpi in the dorsal SVZ (d), just after the HABP decrease. (e) Representative HABP confocal (top) and skeletonized images (bottom) in the dorsal SVZ of sham, 15 and 30 dpi mice. (f) Cumulative distribution of HA skeletons showed a decrease in HA-cables length only in the dorsal SVZ at 7 and 15 dpi. (g) Interconnectivity of the extracellular matrix decreased by 7 dpi in the dorsal SVZ, as measured by fractal dimension. (h) Experimental design for qPCR experiment: 3/4-month mice were subjected to MCAO. Fresh SVZ tissue was extracted 15 and 30 days after MCAO and processed for RT-qPCR analysis. (i) Hyaluronan degradation genes (Hyal1, 2 and 3) increased by 15 and 30 dpi in the SVZ, whereas hyaluronan synthase genes (HAS1 and HAS2) were overexpressed later 30 dpi in the SVZ. Thbs4 and Hif1a genes were also increased by 15 and 30 dpi in the SVZ. Scale bar = 100 µm (a). n = 6 (c, d, e and g) and 3 (i). *$p < 0.05$, **$p < 0.01$ and ***$p < 0.001$ by Krustal Wallis test and Tukey posthoc test (after one-way ANOVA was significant at $p < 0.05$).

SUPPLEMENTARY INFORMATION

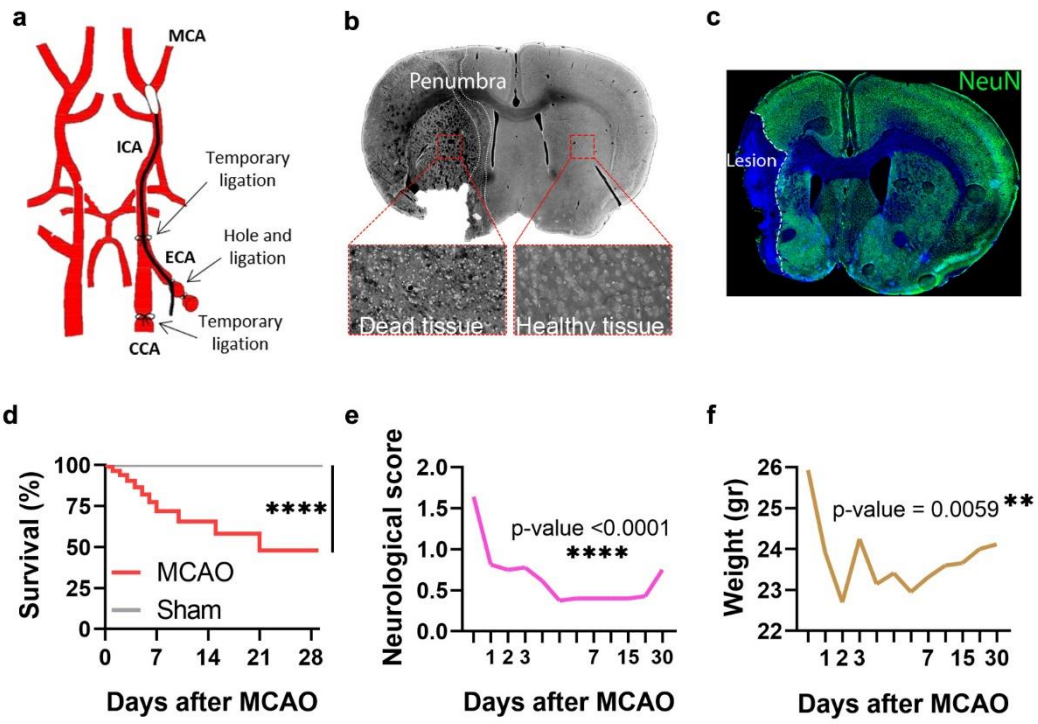

Supplementary Figure 1 – Characterization of the Middle Cerebral Artery Occlusion (MCAO) mouse model of brain ischemia. Related to Figure 2. (a) Scheme of the procedure: 10 mm silicon-coated filament was inserted through an external artery and re-directed to the internal one. Ischemia was induced after 60 minutes of occlusion. After that, the filament was removed, and animals were observed every day before euthanasia. (b) Volume of infarction was observed by cresyl violet staining. (c) Neuronal death was observed by NeuN immunofluorescence. (d) Around 50% of ischemic mice survived at 28 dpi. (e) Ischemic animals ameliorated neurological symptoms overtime. (f) Weight was measured as controls for mice healthcare. n = 17 (d, e, f). **$p < 0.01$ and ****$p < <0.0001$ by survival curve test and Tukey posthoc test (after one-way ANOVA was significant at $p < 0.05$).

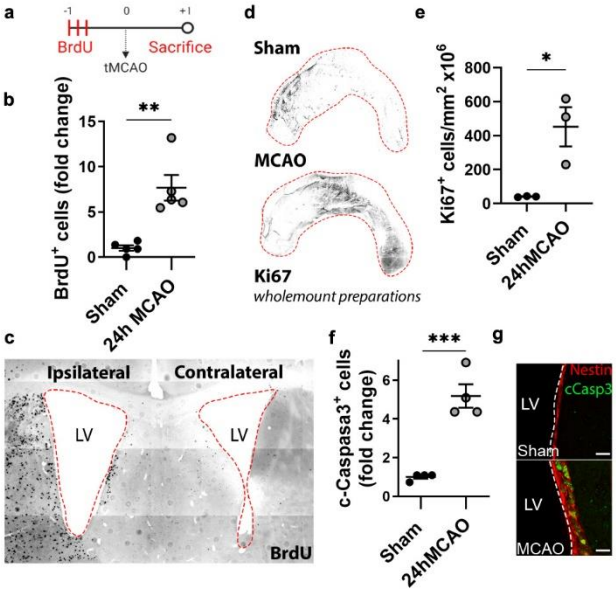

Supplementary Figure 2 – Cell proliferation in the SVZ after brain ischemia. Related to Figure 2. (a) Experimental design: three BrdU (50mg/kg) injections were performed the day before MCAO protocol. Animals were sacrificed 24 hours after the brain stroke model. (b) BrdU positive cells increased in the SVZ 24 hours after MCAO. (c) Representative image of BrdU positive cells in the ipsilateral (left) and contralateral (right) hemisphere 24 hours after MCAO. (d) Ki67 marker was also used to analyze cell proliferation in wholemount preparations of the SVZ. (e) Ki67 positive cells increased in the SVZ 24 hours after MCAO. (f) The Cleaved-Caspase 3 marker increased in the SVZ 24 hours after MCAO. (g) Cleaved-caspase 3 marker was used to assess apoptosis in the SVZ after brain ischemia. Scale bar = 15 µm (g). n = 5 (sham) and 4 (MCAO). Bars represent mean ± SEM. *$p < 0.05$, **$p < 0.01$ and ***$p < 0.001$ by two-tail Student´s t test (sham vs. 24h MCAO).

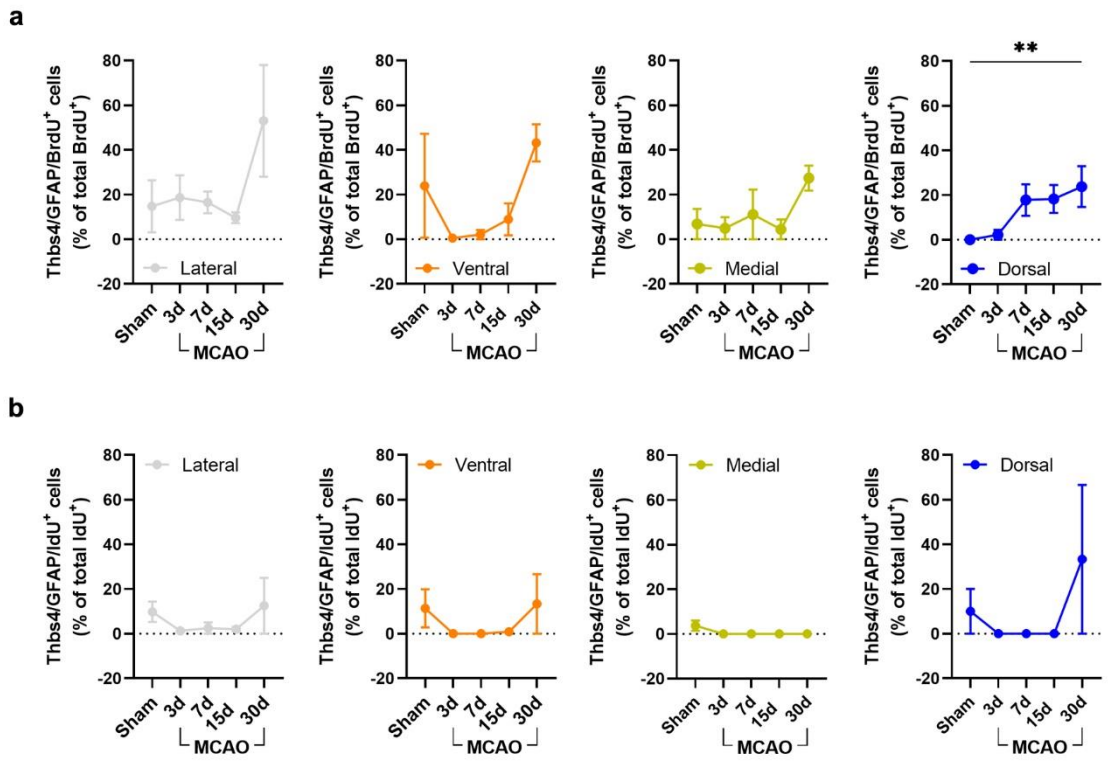

Supplementary Figure 3 – Thbs4 astrocytes derive from slow proliferative cells after brain ischemia. Related to Figure 3. (a) Slow proliferative cells were quantified in the lateral (grey), ventral (orange), medial (yellow) and dorsal (blue) SVZ. We only observed an increase of Thbs4/GFAP/BrdU positive cells in the dorsal SVZ 30 dpi. (b) Thbs4/GFAP/IdU positive cells did not show changes in the lateral (grey), ventral (orange), medial (yellow) and dorsal (blue) SVZ after brain ischemia. n = 4 (sham) and 3 (MCAO). **$p < 0.01$ by by two-tail Student´s t test (sham vs. 30dd MCAO).

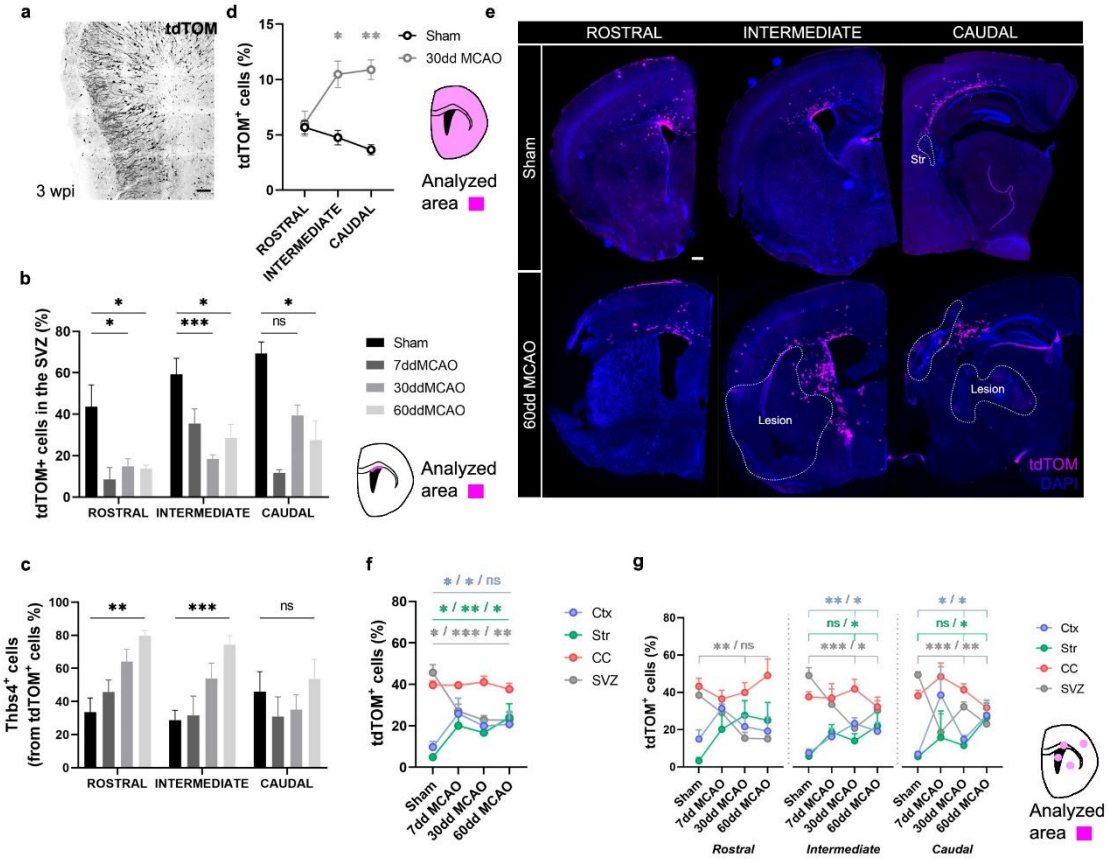

Supplementary Figure 4 – Ischemic-induced Thbs4 astrocytes migrate preferentially to caudal infarcted areas. Related to Figure 4. (a) Representative image of tdTOM positive cells in the OB three weeks after electroporation (3wpi). (b) tdTOM-positive cells decreased in the rostral, intermediate and caudal SVZ 7, 30 and 60 dpi. (c) Thbs4/tdTOM positive cells increased in rostral and intermediate SVZ 30 and 60 dpi. (d) Expression of tdTomato increased in intermediate and caudal brain areas 30 dpi. (e) Representative images of tdTOM expression in rostral (left), intermediate (middle) and caudal (right) brain areas of sham (top) and 60 dpi mice (bottom). (f) tdTOM positive cells increased in the infarcted cortex (Ctx) and striatum (Str) whereas decreased in the dorsal SVZ (SVZ). No changes were observed in the corpus callosum (CC). (g) tdTOM positive cells only increased in the infarcted cortex and striatum at intermediate and caudal brain regions. Scale bar = 100 µm (a) and 1000 µm (e). n = 6 animals per condition. Bars represent mean ± SEM. *$p < 0.05$, **$p < 0.01$ and ***$p < 0.001$ by Dunnett/Tukey posthoc test (after two-way ANOVA was significant at $p < 0.05$).

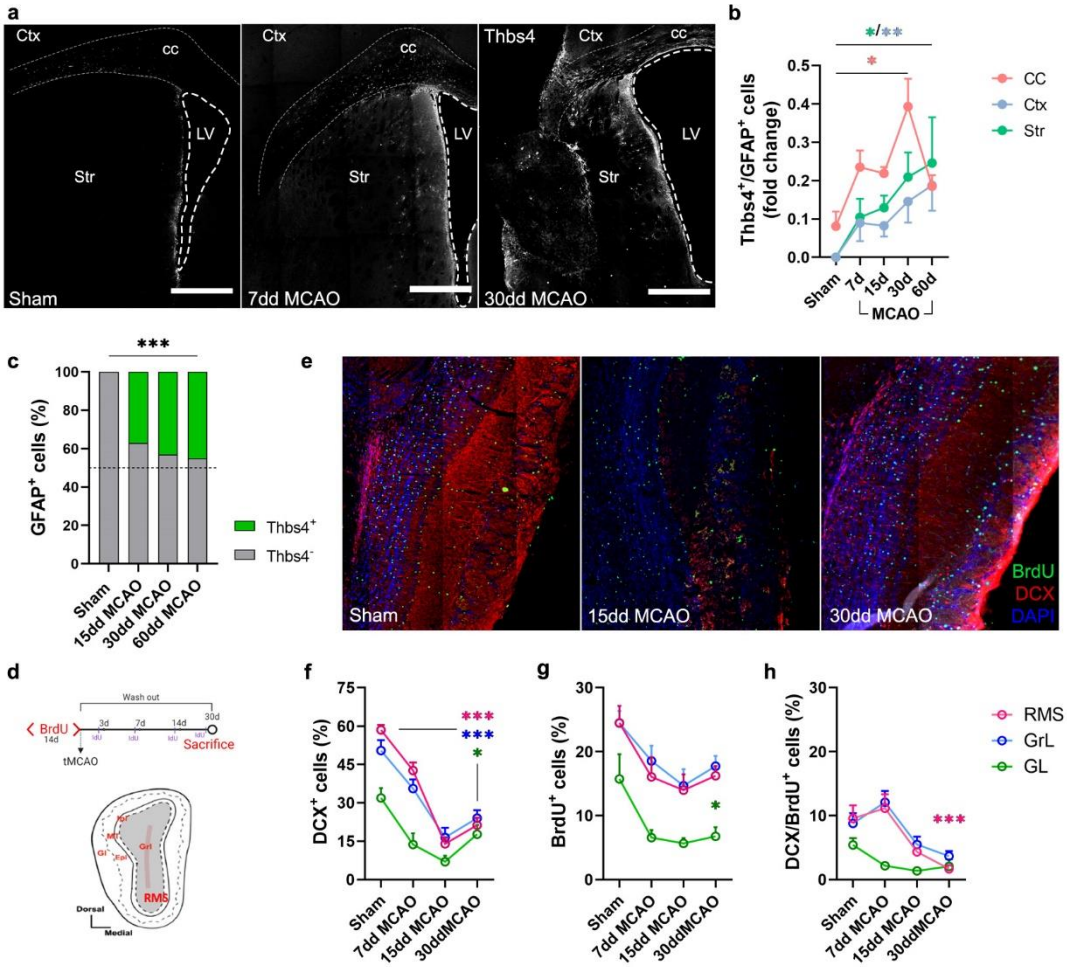

Supplementary Figure 5 – SVZ NSC stop producing newborn neurons to send newborn astrocytes to the ischemic areas. Related to Figure 5. (a) Thbs4 expression in the corpus callosum (cc), infarcted cortex (Ctx) and infarcted striatum (Str) of sham and 7 and 30 dpi mice. (b) Thbs4 increased by 30 dpi in the corpus callosum (cc) and 60 dpi in the infarcted cortex (Ctx) and infarcted striatum (Str). (c) Expression of Thbs4 increased in total GFAP population after 15, 30 and 60 dpi. (d) Experimental design: chronic BrdU (1% in water) treatment was administered for two weeks. BrdU only persisted in slow proliferative NSC (Codega et al., 2014). DCX and BrdU positive cells were measured in the OB layers 7, 15 and 30 dpi. (e) Representative images of BrdU and DCX marker in sham (left), 15 (middle) and 30 (right) dpi mice OB. (f) DCX positive cells decreased 15 and 30 dpi in the RMS, granular OB layer (GrL) and glomerular OB layer (GL). (g) BrdU positive cells only decreased 30 dpi in the glomerular OB layer (GL). Double DCX/BrdU positive cells significative decreased in the RMS 30 dpi. In (f) and (g), values are normalized to total DAPI nuclei (100%). Scale bar = 500 µm (a). n = 6 animals per condition. Lines represent mean ± SEM. *$p < 0.05$, **$p < 0.01$ and ***$p < 0.001$ by Chi-square test and Tukey posthoc test (after two-way ANOVA was significant at $p < 0.05$).

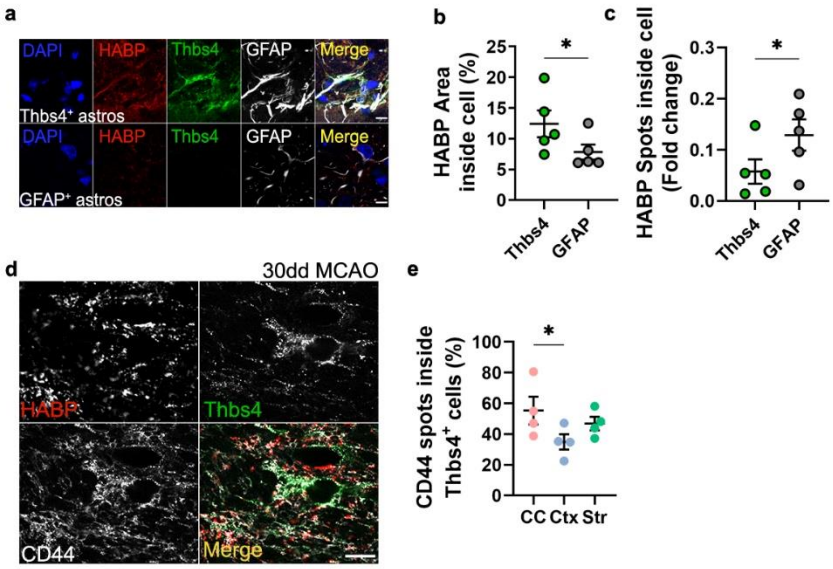

Supplementary Figure 6 – Thbs4 astrocytes internalize HA in the infarcted areas. Related to Figure 6. (a) Representative images of Thbs4/GFAP ("newborn astrocytes", top) and GFAP-only ("local astrocytes", bottom) cells in the infarcted areas 30 dpi. (b) Thbs4-positive astrocytes internalized more HA compare to local astrocytes only labelled with GFAP marker. (c) However, the number of HA spots internalized was higher in local astrocytes compared with Thbs4 astrocytes, suggesting that Thbs4 internalize HA in fewer vesicles. (d) Representative images of HABP (red), Thbs4 (green) and CD44 (white) in the ischemic areas. CD44 is well-known for its role in HA degradation and ECM remodeling. (e) Thbs4 positive astrocytes expressed a high rate of CD44 receptors so much in corpus callosum (CC), infarcted cortex (Ctx) as in infarcted striatum (Str). Scale bar = 10 µm (c, f). n = 5 (b, d and e) and 3 (g) animals per condition. Bars represent mean ± SEM. *$p < 0.05$ and **$p < 0.01$ by Tukey posthoc test (after two-way ANOVA was significant at $p < 0.05$) and two-tail Student´s t test (Thbs4 vs GFAP).

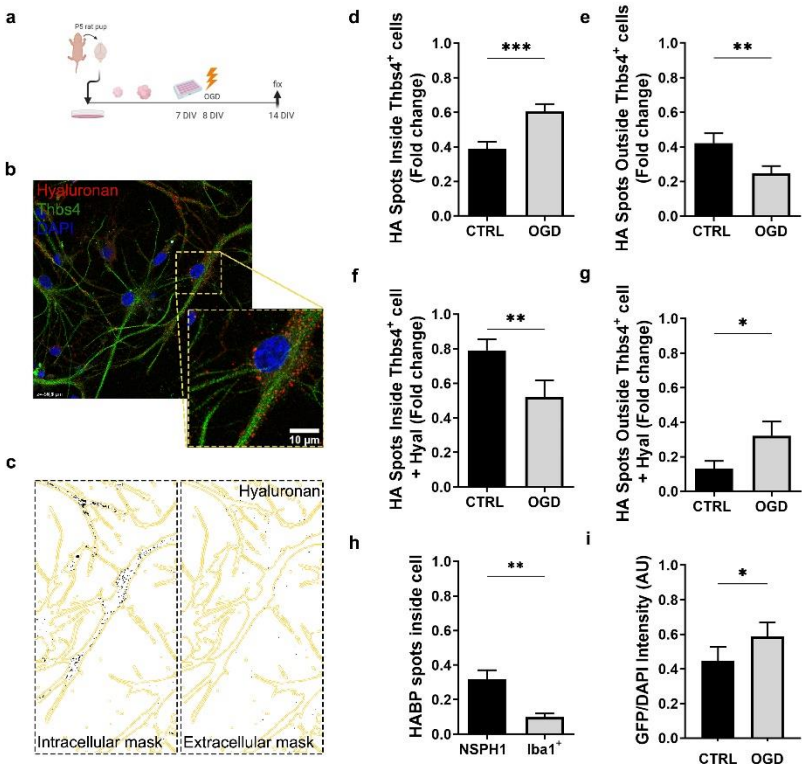

Supplementary Figure 7 – In vitro NSC-derived Thbs4 cells synthetize HA after a hypoxic-ischemic condition. Related to Figure 6. (a) Experimental design: P4 pup rats were sacrificed, and SVZ NSC were extracted and cultured in the proliferative medium for one week. After that, neurospheres were disaggregated and seeded isolated in a culture dish. The following day, oxygen and glucose deprivation protocol (OGD) was performed. Cells were fixed 7 days after culture them. (b) Representative images of in vitro Thbs4 positive cells (green) and HA (red). (c) HA spots were measured inside and outside Thbs4 positive cells. (d) HA spots increased inside Thbs4 positive astrocytes after OGD whereas (e) decreased in the extracellular space. However, when NSC were exposed to hyaluronidases in order to remove extracellular HA, Thbs4 positive cells decreased internalization of HA spots (f) and increased extracellular HA spots (g). (h) Neurosphere-derived NSC (NSPH1) internalized more HA spots compare with Iba1-positive cells. (i) Metalloproteinase activity was higher in OGD NSC cultures compared to control condition. Scale bar = 10 µm (b). n = 15 samples per condition. Bars represent mean ± SEM. *$p < 0.05$, **$p < 0.01$ and ***$p < 0.001$ by two-tail Student´s t test (CTRL vs. OGD; NSPH1 vs. Iba1^{+}).

Table 1. Primary antibodies used for in vivo immunofluorescence protocol

Antibody	Host	Isotope	Dilution	Reference	Company
Thbs4	Mouse	Monoclonal IgM kappa light chain	1/400	Sc-390734	Santa Cruz Biotechnology, USA.
Thbs4	Goat	Polyclonal IgG	1/200	AF2390	R&B systems, USA
S100β	Rabbit	Polyclonal	1/400	Z0311	Dako, Agilent Techonologies, Inc.
S100β	Mouse	Monoclonal IgG2a	1/1000	MA5-12969	Invitrogen, Spain
GFAP	Mouse	Monoclonal IgG1	1/1000	MAB3402	Sigma, Spain
GFAP	Rabbit	Polyclonal	1/4000	Z0334	Dako, Agilent Techonologies, Inc.
βIII tubulin	Rabbit	Polyclonal	1/400	ab18207	Abcam, UK
NeuN	Mouse	Monoclonal IgG1	1/1000	MAB377	Milipore, Germany
DCX	Rabbit	Polyclonal IgG	1/500	ab18723	Abcam, UK
Nestin	Chicken	Polyclonal IgY	1/1000	NES	Aves Lab, EEUU
Prominin 1	Rat	Monoclonal IgG1 kappa	1/300	14-1331-82	Invitrogen, Spain
EGFR	Mouse	Monoclonal	1/400	SAB4200809	Abcam, UK
BrdU	Rat	Monoclonal	1/400	MCA2060	Biorad, USA.
BrdU	Mouse	Monoclonal IgG1, kappa	1/500	03-3900	Invitrogen, Spain
IdU	Mouse	Monoclonal IgG2b	1/100	MA5-24879	Invitrogen, Spain
Ki67	Rabbit	Polyclonal IgG	1/400	Ab15580	Abcam, UK
Cleaved-Caspase 3	Rabbit	Monoclonal IgG	1/300	#9664	Cell Signaling, Germany
CD44	Rat	Monoclonal IgG2b	1/500	MA517875	Invitrogen, Spain
FLAG	Mouse	Monoclonal IgG1	1/500	F1804	Sigma, Spain
Olig2	Mouse	Monoclonal IgG2aκ	1/1000	MABN50	Milipore, Germany

Table 2. Primer sequences for qPCR

Name	Sequence
Hyal1_FW	GTGCCAAGCCCTATGCTAATAAG
Hyal1_REV	GCATGTCCATTGCAAAGACTGA
Hyal2_FW	GTCCCACATACACCCGAGGA
Hyal2_REV	GGCACTCTCACCGATGGTAGA
Hyal3_Ffw	GGACGACCTGATGCAGACTATTG
Hyal3_REV	GGTCCCCCCAGAGTACCACT
Has1_FW	AGGGCTCTTAAAGGAGGAGTCC
Has1_REV	AGAAGGTAAACTGAGTCCCCAGAA
Has2_FW	CAAAGAGGTTCGTTCAAGTTCTGA
Has2_REV	TGTGTTTGTTTCCCACTAGCTCTC
Hif1a_FW	CATAAAGTCTGCAACATGGAAGGT
Hif1a_REV	ATTTGATGGGTGAGGAATGGGTT
HPRT1_FW	TGATAGATCCATTCCTATGACTGTAGA
HPRT1_REV	AAGACATTCTTTCCAGTTAAAGTTGAG